



*AGU Advances*

First Revision of

**The Chicxulub Impact Produced a Powerful Global Tsunami**

Molly M. Range<sup>1\*</sup>, Brian K. Arbic<sup>1,2</sup>, Brandon C. Johnson<sup>3,4</sup>, Theodore C. Moore<sup>1</sup>, Vasily Titov<sup>5</sup>, Alistair J. Adcroft<sup>6</sup>, Joseph K. Ansong<sup>1,7</sup>, Christopher J. Hollis<sup>8</sup>, Jeroen Ritsema<sup>1</sup>, Christopher R. Scotese<sup>9</sup>, and He Wang<sup>1,10,11</sup>

<sup>1</sup> Department of Earth and Environmental Sciences, University of Michigan, Ann Arbor, MI 48109, USA

<sup>2</sup> Recently on sabbatical at Institut des Géosciences de L'Environnement (IGE), Grenoble, France, and Laboratoire des Etudes en Géophysique et Océanographie Spatiale (LEGOS), Toulouse, France

<sup>3</sup> Department of Earth, Atmospheric, and Planetary Sciences, Purdue University, West Lafayette, IN 47907, USA

<sup>4</sup> Department of Physics and Astronomy, Purdue University, West Lafayette, IN 47907, USA

<sup>5</sup> National Oceanic and Atmospheric Administration, Pacific Marine Environmental Lab, Seattle, WA 98155, USA

<sup>6</sup> Atmospheric and Oceanic Sciences Program, Princeton University, Princeton, NJ 08540, USA

<sup>7</sup> Department of Mathematics, University of Ghana, P.O. Box LG 62, Legon, Accra, Ghana

<sup>8</sup> School of Geography, Environment and Earth Sciences, Victoria University of Wellington, New Zealand

<sup>9</sup> PALEOMAP Project, 134 Dodge, Evanston, IL 60202, USA

<sup>10</sup> Oceanic and Atmospheric Administration, Geophysical Fluid Dynamics Laboratory, Princeton, NJ 08540, USA

<sup>11</sup> University Corporation for Atmospheric Research, P.O. Box 3000, Boulder, CO 80307-3000

# 1 The Chicxulub Impact Produced a Powerful Global Tsunami

2 **Molly M. Range**<sup>\*1</sup>, **Brian K. Arbic**<sup>1,2</sup>, **Brandon C. Johnson**<sup>3,4</sup>, **Theodore C. Moore**<sup>1</sup>, **Vasily Titov**<sup>5</sup>,  
3 **Alistair J. Adcroft**<sup>6</sup>, **Joseph K. Ansong**<sup>1,7</sup>, **Christopher J. Hollis**<sup>8</sup>, **Jeroen Ritsema**<sup>1</sup>, **Christopher R.**  
4 **Scotese**<sup>9</sup>, and **He Wang**<sup>1,10,11</sup>

5  
6 <sup>1</sup>Department of Earth and Environmental Sciences, University of Michigan, Ann Arbor, MI, 48109, USA;  
7 <sup>2</sup>Recently on sabbatical at Institut des Géosciences de L'Environnement (IGE), Grenoble, France, and  
8 Laboratoire des Etudes en Géophysique et Océanographie Spatiale (LEGOS), Toulouse, France;  
9 <sup>3</sup>Department of Earth, Atmospheric, and Planetary Sciences, Purdue University, West Lafayette, IN 47907,  
10 USA; <sup>4</sup>Department of Physics and Astronomy, Purdue University, West Lafayette, IN 47907, USA;  
11 <sup>5</sup>National Oceanic and Atmospheric Administration, Pacific Marine Environmental Lab, Seattle, WA  
12 98155, USA; <sup>6</sup>Atmospheric and Oceanic Sciences Program, Princeton University, Princeton, NJ 08540,  
13 USA; <sup>7</sup>Department of Mathematics, University of Ghana, P.O. Box LG 62, Legon, Accra, Ghana; <sup>8</sup>School  
14 of Geography, Environment and Earth Sciences, Victoria University of Wellington, New  
15 Zealand; <sup>9</sup>PALEOMAP Project, 134 Dodge, Evanston, IL 60202, USA; <sup>10</sup>National Oceanic and  
16 Atmospheric Administration, Geophysical Fluid Dynamics Laboratory, Princeton, NJ 08540, USA;  
17 <sup>11</sup>University Corporation for Atmospheric Research, P.O. Box 3000, Boulder, CO, 80307-3000

18 Corresponding author: Molly Range ([mmrange@umich.edu](mailto:mmrange@umich.edu))

## 19 Key Points:

- 20
- 21 • The authors present the first global simulation of the Chicxulub impact tsunami
  - 22 • Total energy present in the impact tsunami is much greater than for any modern-day tsunami
  - 23 • Impact tsunami flow velocities are strong enough to disturb and erode sediment in basins halfway around the globe

## 24 Abstract

25 The Chicxulub crater is the site of an asteroid impact linked with the Cretaceous-Paleogene (K-Pg) mass  
26 extinction at ~66Ma. This asteroid struck in shallow water and caused a large tsunami. Here we present the  
27 first global simulation of the Chicxulub impact tsunami from initial contact of the projectile to global  
28 propagation. We use a hydrocode to model the displacement of water, sediment, and crust over the first ten  
29 minutes, and a shallow-water ocean model from that point onwards. The impact tsunami was up to 30,000  
30 times more energetic than the December 26, 2004 Indian Ocean tsunami, one of the largest tsunamis in the  
31 modern record. Flow velocities exceeded 20 cm/s along shorelines worldwide, as well as in open-ocean  
32 regions in the North Atlantic, equatorial South Atlantic, southern Pacific and the Central American  
33 Seaway, and therefore likely scoured the seafloor and disturbed sediments over 10,000 km from the impact  
34 origin. The distribution of erosion and hiatuses in the uppermost Cretaceous marine sediments are  
35 consistent with model results.  
36

## 37 Plain Language Summary

38  
39 At the end of the Cretaceous, about 66 million years ago, the Chicxulub asteroid impact near the Yucatan  
40 peninsula produced a global tsunami 30,000 times more energetic than any modern-day tsunami produced  
41 by earthquakes. Here we model the first ten minutes of the event with a crater impact model, and the  
42 subsequent propagation throughout the world oceans using two different global tsunami models. The  
43 Chicxulub tsunami approached most coastlines of the North Atlantic and South Pacific with waves of over

44 10 meters high and flow velocities in excess of 1 m/s offshore. The tsunami was strong enough to scour  
45 the seafloor in these regions, thus removing the sedimentary records of conditions before and during this  
46 cataclysmic event in earth history and leaving either a gap in these records or a jumble of highly disturbed  
47 older sediments. The gaps in sedimentary records generally occur in basins where the numerical model  
48 predicts larger bottom velocities.

49  
50

## 51 **1 Introduction**

52 The impact of an approximately 14-km diameter asteroid is implicated in the Cretaceous/Paleogene (K-Pg)  
53 mass extinction (Schulte et al., 2010) approximately 66 Ma ago. The bolide impact caused global  
54 temperature fluctuations (Schulte et al., 2010), large aerosol plumes (Bardeen et al., 2017), large plumes of  
55 soot and dust (Brugger et al., 2017), wildfires from ejecta re-entering the atmosphere (Busby et al., 2002;  
56 Morgan et al., 2013), and a massive tsunami (Matsui et al., 2002; Kinsland et al., 2021). Drilling cores  
57 from the Integrated Ocean Drilling Program (Gulick et al., 2016) and the International Continental Drilling  
58 Program (ICDP) corroborated the models (Collins et al., 2008) of the exact physical and geophysical  
59 nature of the crater and its peak ring which has facilitated detailed modeling of the impact (Morgan et al.,  
60 2016). Earlier tsunami simulations described the effects of the tsunami within the confines of the Gulf of  
61 Mexico (e.g., Ward, 2012; Matsui et al., 2002; see Ward, 2021 for a more recent simulation extending  
62 beyond the Gulf of Mexico). Subsequent submarine landslides on the marine shelf (Gulick et al., 2008)  
63 could potentially increase the energy of this tsunami.

64

65 Most global tsunami simulations to date have been of tsunamis induced by underwater earthquakes, for  
66 instance, the 2004 Indian Ocean tsunami (Smith et al., 2005, Titov et al., 2005). Tsunami propagation has  
67 traditionally been simulated with shallow-water ocean models, which assume hydrostatic water pressure  
68 and a small depth-to-wavelength ratio. Such models cannot be used to simulate the complex first ten  
69 minutes of the Chicxulub impact tsunami when there was large-scale deformation of the crust and the  
70 formation of a crater (Morgan et al., 2016). The crater formation and post-impact ejecta splashing back  
71 into the ocean create highly non-linear and non-hydrostatic waves. Modeling the impact tsunami requires a  
72 multi-stage simulation, with hydrocode modeling of crater formation and post-impact non-hydrostatic  
73 water waves, before hand-off of the solution to global shallow-water models. We pursue such a two-stage  
74 strategy in this paper.

75

76 These linked models seek to depict a complex set of events associated with the asteroid impact and to  
77 predict the pathways of propagation as applied to a world with very different sea levels, ocean gateways,  
78 and continental positions and boundaries. The models do not incorporate a description of the chaotic near-

79 field tectonic disturbances (e.g., faulting and slope failures) and the generation of smaller tsunamis by  
80 these disturbances. Did these aspects of the impact event alter the strength or the propagation pathway of  
81 the impact tsunami, or was this tsunami so large and so powerful that these other effects were masked and  
82 overpowered? To verify the modeled strength and pathways taken by the impact tsunami we look at a  
83 global array of K-Pg boundary intervals in marine sections on land and in ocean drilling cores. In these  
84 sites we will look for documented evidence of erosion, sediment disturbance, and/or redeposition of  
85 sediments that can be reasonably associated with the impact tsunami.

86

## 87 **2 Impact Modeling**

### 88 **2.1 Methods**

89 We use the axisymmetric iSALE-2D hydrocode (Collins et al., 2004; Wünnemann et al., 2006) to simulate  
90 the initial formation of the Chicxulub impact tsunami. iSALE-2D has been used to simulate impact-  
91 induced tsunamis (e.g., Weiss et al., 2006; Weiss and Wünnemann, 2007; Wünnemann et al., 2010). The  
92 results of our iSALE-2D simulations were used to create initial conditions for shallow-water models to  
93 trace the tsunami throughout the world's ocean.

94

95 Motivated by impact simulations that reproduce the seismically imaged structure of Chicxulub (Collins et  
96 al., 2008) as well as the peak shock pressures and composition of the basin's peak-ring, as constrained by  
97 recent drilling (Morgan et al., 2016), we assume that the 14-km-diameter impactor had a density of 2650  
98 kg/m<sup>3</sup> and struck Chicxulub at 12 km/s. Although the Chicxulub impact is thought to be oblique (45-60  
99 degrees from horizontal; Collins et al., 2020; Robertson et al., 2021) the axisymmetric nature of the code  
100 limits us to simulation of vertical impacts. We expect this limitation to have a minor effect on our results  
101 as the formation of the outward propagating rim wave (more below) is dominated by emplacement of slow  
102 ejecta that tends to be symmetric (e.g., Anderson et al., 2003). Our simulations have the same setup as  
103 those in Collins et al. (2008), but with a finer grid spacing and a larger domain needed to track the  
104 formation and early evolution of the tsunami (see SI Table 1 and other material in Supporting Information;  
105 hereafter referred to as SI). We model the target as a granitic crust overlain by a 4-km-thick layer of  
106 sediments and an ocean with a constant depth of 1, 2, or 3 km (a 2-km ocean depth was used by Collins et  
107 al. (2008) for the northwestern sector of Chicxulub). With a grid resolution of 100 m, the ocean depth is  
108 resolved by 10, 20, and 30 cells, respectively, depending on assumed ocean depths of 1, 2, and 3 km. This  
109 number of grid cells is sufficient to resolve the rim wave (Bahlburg et al., 2010; SI). The atmosphere is not  
110 expected to significantly affect the early propagation of the tsunami. Thus, we do not include the

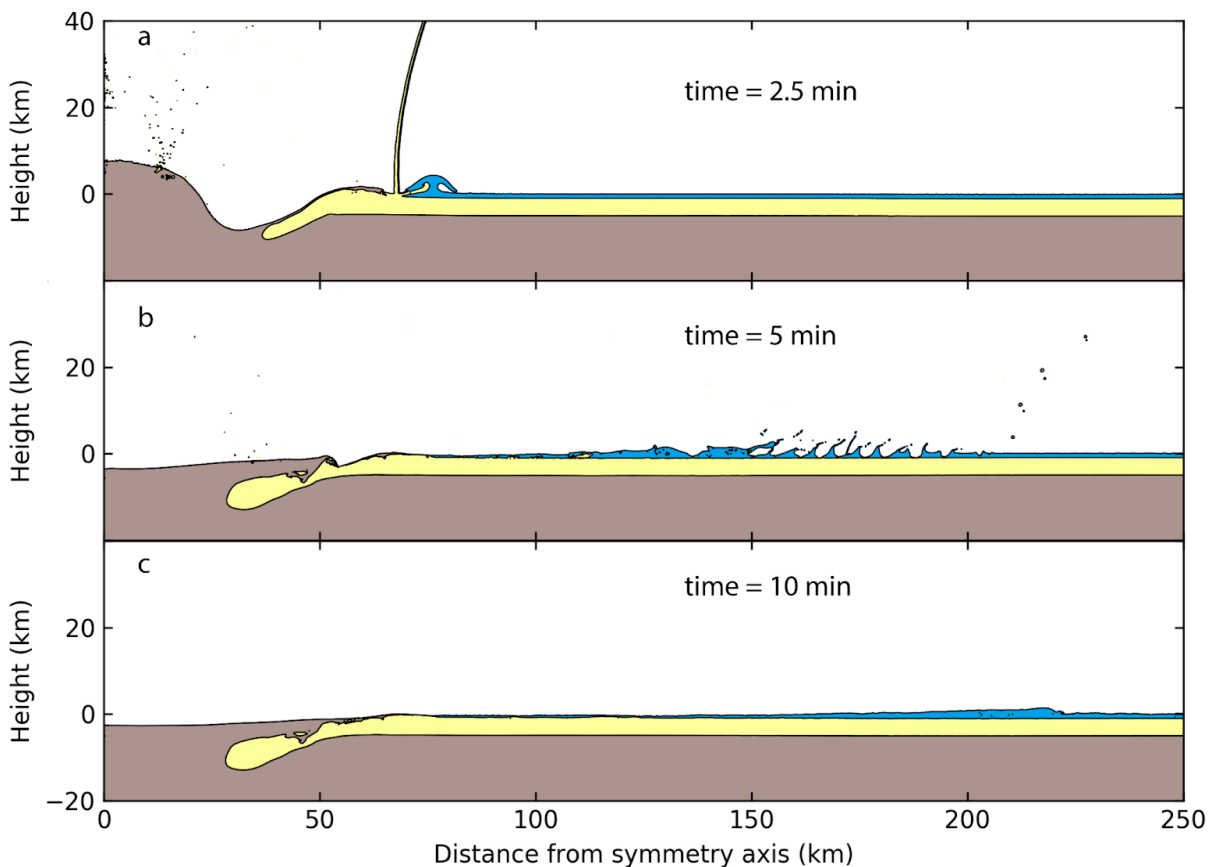
111 atmosphere in our simulations. Further details of the iSALE simulations used in this paper, and their  
112 sensitivities to grid spacing, can be found in SI.

113

## 114 2.2 Results

115 The dimensions and formation of the crater are similar to previous work (Collins et al., 2008; Morgan et  
116 al., 2016). The results of our “fiducial” hydrocode impact simulation, with an assumed seafloor depth of 1  
117 km and a run time of 10 minutes, are shown in Figure 1. About 2.5 minutes after contact of the projectile,  
118 a curtain of ejecta pushing water outward from the impact produced a 4.5-km-high wave (Fig. 1a). After 5  
119 minutes, falling ejecta continued to impart momentum to the ocean (Fig. 1b). At 10 minutes, after all the  
120 ejecta had fallen, a 1.5-km-high wave, known as a rim wave, located 220 km from the point of impact was  
121 left propagating throughout the deep ocean (Fig. 1c).

122



123

124 **Figure 1.** Formation of Chicxulub crater and the associated tsunamis. Time series with material colored  
125 according to material type (crustal material is brown, sediments are yellow, and the ocean is blue). The  
126 origin marks the point of impact. Black curves mark material interfaces (e.g., sediment-crust interface).  
127 An animation of these results, from 0 to 10 minutes in steps of 5 seconds, is shown in SI Video 1.

128

129 The axisymmetric nature of our high-resolution hydrocode model requires an ocean layer with a constant  
130 water depth. The ocean depth at the point of impact is estimated to be 100-200 m (Gulick et al. 2008) and  
131 becomes deeper toward the northwest. Generation of the tsunami rim wave, however, is sensitive to the  
132 ocean depth at the crater rim, not at the point of impact. Paleobathymetry estimates indicate that water  
133 depth was ~1 km where ejecta emplacement produces the initial rim-wave (50 km from basin center). At  
134 ~150 km from the point of impact the ocean was ~3 km deep (SI Fig. 1). To test for sensitivity of the rim  
135 wave and crater shape to pre-impact ocean depth we vary the thickness of the ocean layer from 1 to 3  
136 km. The waveforms after the first 10 minutes of the fiducial simulation, and after the first 10 minutes of  
137 iSALE simulations with different water depths, are displayed in Figure 2. These waveforms are in good  
138 agreement with the waveforms found in Bahlburg et al. (2010). SI Fig. 4 demonstrates that handoff to  
139 MOM6 at 600 s and 850 s give nearly identical globally integrated energies. Surprisingly, the crater and  
140 rim wave structure at these early times do not depend strongly on assumed ocean depth within the range of  
141 1-3 km. We do not expect this weak dependence to hold over much deeper or shallower ocean  
142 depths. Our two-dimensional axisymmetric model with a constant depth is clearly a simplification of the  
143 bathymetry in the Gulf of Mexico. In the case of the 1 km ocean depth simulation, a sediment rim on the  
144 impact crater ten minutes into the run rose above the water column, creating a ring-shaped island. As the  
145 rim was composed of loose sediment, it would likely have been quickly dispersed by wave action (Bell et  
146 al., 2004). Other authors however have argued that resurgence of water into the crater occurred by penetration  
147 through the raised rim and erosion allowing flow at locations along the rim (Bahlburg et al. 2010). To test  
148 for sensitivity to this uncertainty, we model one initial condition with a sediment rim and one without. We  
149 test for sensitivity between the two runs and found the tsunami energies to be comparable (not  
150 shown). Therefore, the 1 km water depth iSALE simulation, with no sediment rim, is used for all  
151 subsequent runs.

152

### 153 **3 Tsunami Propagation Modeling**

#### 154 **3.1 Methods**

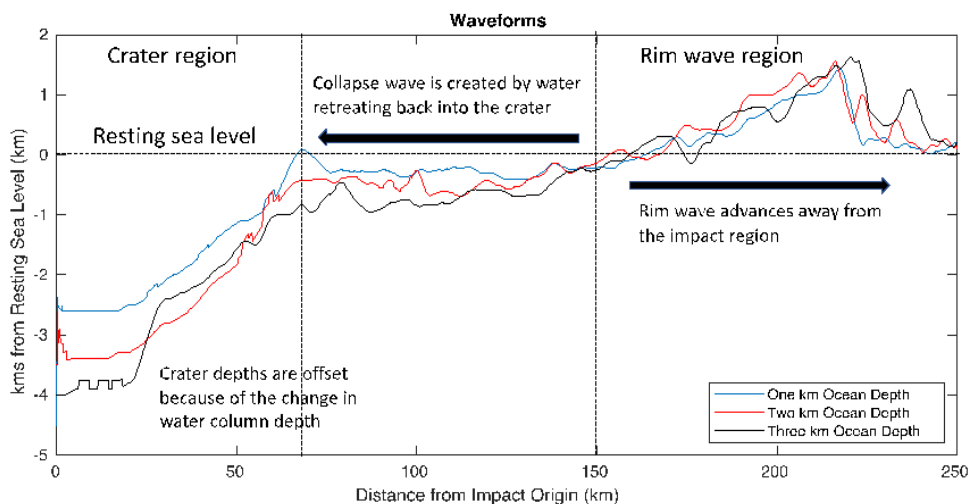
155 To simulate the global propagation of the impact tsunami, we use two different well-established shallow-  
156 water models: the Geophysical Fluid Dynamics Laboratory (GFDL) Modular Ocean Model Version 6  
157 (Adcroft, 2017; MOM6), and Methods Of Splitting Tsunamis (Titov et al, 2016; MOST). The rim-wave  
158 has a wavelength of about 50-100 km, similar to the wavelengths seen in the 2004 Indian Ocean  
159 tsunami. As this is much greater than average ocean depths of about 4 km, the shallow water assumption,  
160 which assumes hydrostatic balance and is based on a comparison of wavelengths vs. water depth, is well  
161 satisfied. The similarity of simulations from two different models using the same underlying shallow-water

162 approximation and run on the same 1/10<sup>th</sup> degree grid but differing in their respective numerical  
163 implementations (more below) ensures robustness of our results.

164

165 Shallow-water models solve for perturbations to the resting sea surface elevations and for depth-averaged  
166 flow velocities. Flow velocities are the velocities of particles in the water, in contrast to the phase  
167 velocities of the tsunami wave propagating throughout the ocean. The hydrostatic approximation will  
168 modify the wave speed. Errors due to this approximation are likely less than errors due to uncertainties in  
169 bathymetry. The large amplitudes of impact-generated waves lead to nonlinear dynamics during  
170 propagation, which is described only approximately by the shallow-water wave theory. Nevertheless, the  
171 long wave approximations have been successfully applied for simulating the nonlinear tsunami dynamics  
172 of propagation in shallow coastal regions and runup. Synolakis et al. (2008), for example, include an  
173 extensive discussion of verification and validation of shallow-water tsunami models with respect to field  
174 benchmarks. Their study demonstrates that large-amplitude waves can be predicted accurately with the  
175 shallow-water wave theory, providing the long wave assumption is valid.

176



177

178 **Figure 2.** Waveform and crater shape for three different runs from the iSALE-2D hydrocode. In the left-  
179 most part of the plot, the crater depths are shown. The middle and right-parts of the plot follow the change  
180 in sea level relative to the resting sea level. The crater depths are displaced by about one km from each  
181 other because of the differing ocean depths of the three runs.

182

183 MOM6 has been used to model tsunamis in the deep ocean, although it has not been used to forecast  
184 tsunamis. The barotropic solver in MOM6 is based on the solver in the Hallberg Isopycnal Model  
185 (HIM)/Generalized Ocean Layered Model (GOLD), which were used in the tsunami studies of Smith et al.  
186 (2005) and Kunkel et al. (2006). The results in Adcroft (2013) suggest that deep-ocean, large-scale

187 motions are not overly sensitive to the horizontal resolution of the model. The "forecasting" accuracy of  
188 the tsunami calculation is not relevant for the application of the Chicxulub impact tsunami, but at 1/10<sup>th</sup>  
189 degree global resolution the arrival times are accurate to about 1%.

190

191 MOST was developed specifically for tsunami simulations (Titov & Synolakis, 1995; Titov et al.,  
192 2016). MOST has been extensively tested for various tsunami modeling applications and has been used to  
193 simulate historical tsunamis of different origins, including modeling of global tsunami propagation and  
194 local tsunami inundation impacts. MOST is now used operationally for tsunami forecasts at NOAA  
195 Tsunami Warning Centers. While MOM6 is run for all of the cases shown in this paper, MOST is run  
196 only in the fiducial case described below.

197

198 Both tsunami propagation models used the same global 1/10<sup>th</sup> degree bathymetric grid (SI Tables 2 and 3).  
199 To accurately simulate tsunami propagation, a global Maastrichtian (66Ma) paleobathymetry is combined  
200 with the initial condition from the hydrocode results. The sources for the global paleobathymetry are  
201 Müller et al. (2008) and Scotese (1997). More information about the bathymetries that we used, and the  
202 manner in which we combined them, can be found in SI Text S1.

203

204 To continue the simulation with the tsunami propagation codes we convert the axisymmetric, constant  
205 water depth hydrocode results (see SI Figure 2) to more realistic, non-axisymmetric conditions with  
206 horizontally varying resting water depths. The hydrocode results at 600 seconds post-impact were used for  
207 the shallow-water model initial condition. At this time there was no more resolved falling ejecta; less  
208 voluminous and potentially fine ejecta would continue to fall after 600 s, but we do not expect that this  
209 more distal ejecta would significantly affect the rim wave. At 600 s, there is a defined waveform of  
210 perturbation sea surface heights, in approximate hydrostatic balance because the wavelength is much  
211 greater than the water depth (see Fig. 2). The waveform, crater shape and velocity are isolated from the  
212 density profile. Assuming radial symmetry, the waveform is converted into a ring-shaped outward  
213 propagating wave, dependent on resting sea level, and inserted into the paleobathymetry described  
214 above. In the bathymetry the crater extended onto land where water was not initially present before  
215 impact. We test having a crater purely in water, without the portion of the crater that is formed over land  
216 ('Half Crater'), as well as a more complete crater that extended a full 360° onto land, ('Full Crater'), and  
217 compare energies, as discussed further below. The fiducial model employs the 'Half Crater' bathymetry.  
218 More information on the blending of the hydrocode results into the paleobathymetry is given in SI.

219



220 To test sensitivity to the horizontal grid spacing of the shallow-water model, we run a shallow-water  
221 simulation at  $1/5^\circ$  grid spacing and compare snapshots of two-dimensional sea surface height perturbation  
222 fields (SI Fig. 3) and energies (SI Fig. 4) between this run and the nominal  $1/10^\circ$  run. To test for the  
223 sensitivity of the transfer point (“hand-off”) between the hydrocode and ocean model, we run a hydrocode  
224 simulation, with a larger mesh, out to 850 seconds before emplacement of the hydrocode conditions in the  
225 MOM6 model. More details can be found in SI.

226

### 227 **3.2 Results**

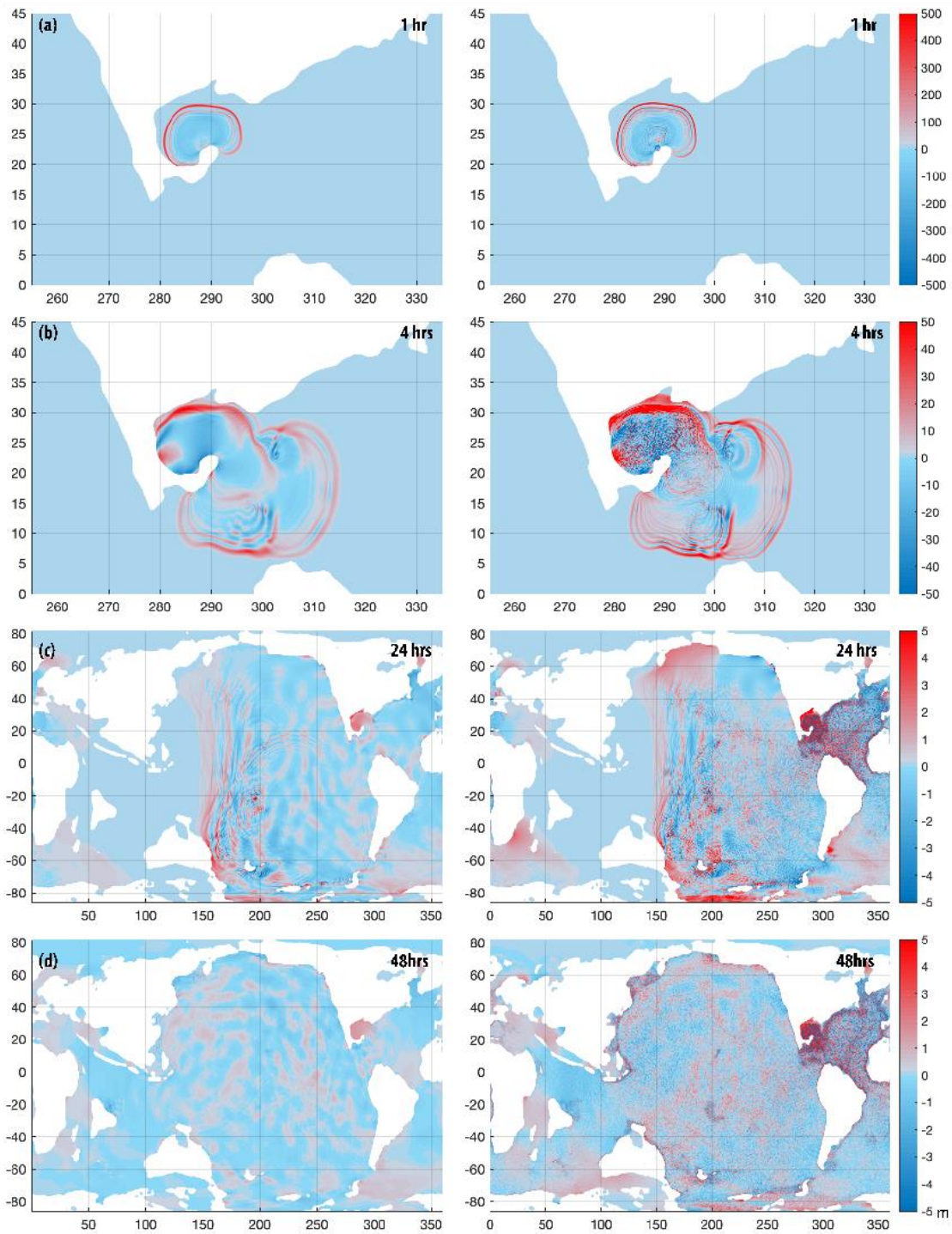
228 Both shallow-water propagation models are run using the same fiducial run initial conditions and  
229 bathymetry data. Snapshots of the MOM6 and MOST sea surface amplitudes are compared at the same  
230 times to ensure consistency of the results. The models display similar tsunami propagation patterns (Fig.  
231 3). The main dissimilarities in the model behaviors are in the later-stage wave dynamics. The differences  
232 reflect different numerical implementation of the shallow-water wave equations used in the two models.  
233 MOST is using the Godonov-type method (a Riemann solver) with a directional splitting, which  
234 emphasizes wave characteristics, and a discretization of non-linear terms in Lagrangian form. MOM6  
235 employs vector invariant equations using an energy conserving discretization, with an emphasis on a well-  
236 behaved spectra in a turbulent cascade (not resolved or relevant to this problem). In addition, the bottom  
237 dissipation is parameterized differently in the two models. MOM6 displays more short-wavelength  
238 features after the initial, highest amplitude wave passing. Additional differences arise from different  
239 treatments of the north and south boundaries by MOM6 (reflecting boundaries) and MOST (absorbing  
240 boundaries without reflection). These model differences do not affect the leading order wave  
241 dynamics. The impact tsunami spread outside the Gulf into the Atlantic after about one hour from impact  
242 (Fig. 3a); after 4 hours, through the Central American seaway, the waves enter into the Pacific (Fig. 3b);  
243 after 24 hours of propagation, the waves cross most of the Pacific from the east and Atlantic from the west  
244 and entered the Indian Ocean from both sides (Fig. 3c). The tsunami front propagates in excess of 200 m/s  
245 in deep water, in accordance with the shallow-water celerity. By 48 hours post-handoff, e.g., 48 hours  
246 after the handoff from the hydrocode to the shallow-water model, significant tsunami amplitudes have  
247 reached most of the world coastlines creating a complex amplitude pattern due to wave reflection and  
248 refraction (Fig. 3d). Due to wave shoaling the open ocean amplitudes can multiply many-fold near  
249 coastlines. The open-ocean amplitudes in most of the Gulf of Mexico are computed to be over 100  
250 m. Along many North Atlantic coastal regions and some South America Pacific coastal regions the  
251 models show over 10 m offshore amplitudes. The simulations predict that most of the world ocean  
252 experiences maximum offshore amplitudes above 1 m, with the exception of some areas in the Indian

253 Ocean and Mediterranean. Any historically documented tsunamis pale in comparison with such global  
254 impact. Depending on the geometries of the coast and the advancing waves, most coastal regions would be  
255 inundated and eroded to some extent. The simulations used here do not include wave run-up onto land, as  
256 the model resolution of  $1/10^\circ$  is too low to resolve details of the inundation dynamics.

257

258 The maximum wave amplitudes and flow velocities (current speeds) at each model grid cell, over the two-  
259 day time period of the MOST simulation, are respectively shown in Figs. 4a and 4b. The largest waves  
260 and current speeds are in the Gulf of Mexico, North Atlantic, and South Pacific. Near the point of impact,  
261 the flow velocity exceeds 100 m/s. In other basins, flow velocities are up to a factor of 100 times smaller  
262 in the middle of the ocean than they are near the impact origin and along the coasts. Flow velocities above  
263 20 cm/s are expected to cause erosion of fine-grained pelagic sediments (Lonsdale and Southard, 1974;  
264 McCave, 1984). Velocities higher than 20 cm/s are predicted in offshore areas of the North Atlantic and  
265 the equatorial region of the South Atlantic, in the Central American seaway and in most of the southern  
266 and southwestern Pacific, more than 12,000 km from the impact area. Most coastal areas of the world  
267 experienced above-20-cm/s velocities. As discussed in SI, tsunami propagation and flow velocities of  
268 simulations with slightly different input configurations (varying model resolution, friction coefficients,  
269 hand-off times between hydrocode and shallow-water models, crater size, etc.) are also tested for  
270 sensitivity. The energy of the tsunami is not greatly changed in any of these sensitivity tests except for the  
271 case in which the rim wave is removed.

272



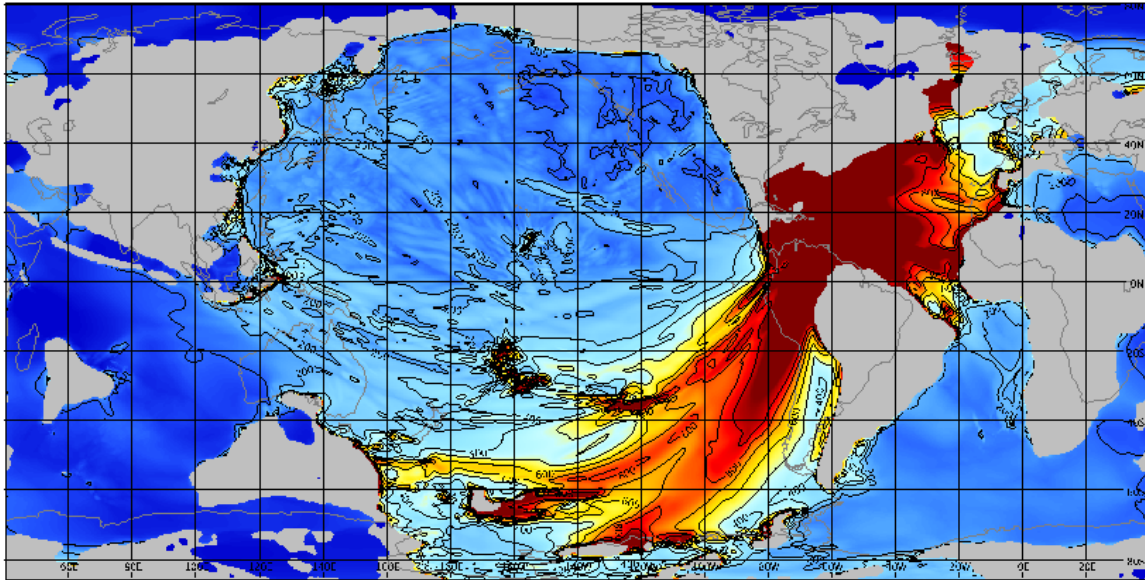
273

274

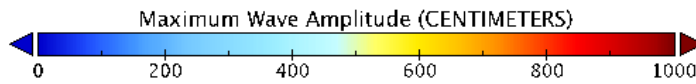
275 **Figure 3.** Comparison of two tsunami propagation models: MOST model – left column, MOM6 – right  
 276 column. Sea surface height perturbation in meters shown at 1 hour (a) and 4 hours (b) after impact around  
 277 Gulf of Mexico, 24 hours (c) and 48 hours (d) post-handoff globally. Animations for both models are  
 278 provided in SI Videos 3 and 4.

279

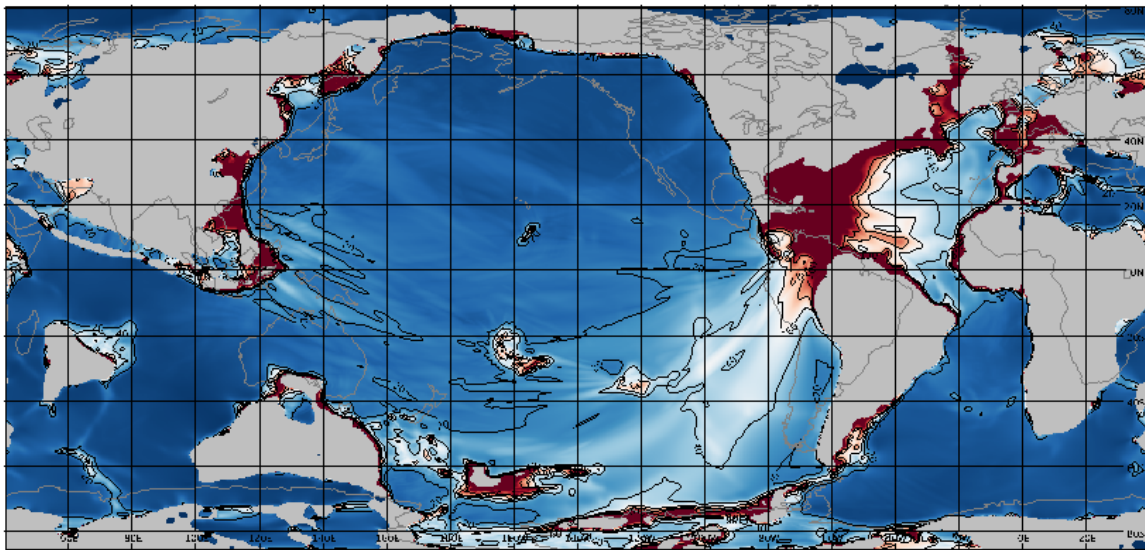
### Maximum Wave Amplitude



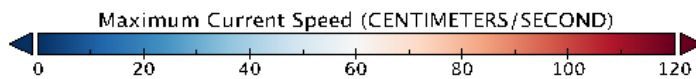
(a)



### Maximum Current Speed



(b)



280

281

282

283

284

285

**Figure 4.** Maximum tsunami sea surface perturbation heights (a) and maximum flow velocity (b) at each grid cell. Contours are shown for every meter of amplitude (saturated at 1000 cm) and every 20 cm/s of speed. Contours of modern continents are shown for reference as gray lines. The results of the MOST model are shown here, because MOST saves values more frequently than MOM6. The results, however, are similar for both models.

## 286 4. Geologic Verification of the Models

### 287 4.1 Methods

288 Identifying the K-Pg boundary in marine sections requires some form of stratigraphic information. This is  
289 usually provided by biostratigraphic or paleomagnetic investigations. Marine sections located above  
290 present-day sea level and exposed on land usually allow a broad view of boundaries in outcrop and  
291 extensive stratigraphic data can often be collected from the section. Based on these studies and the overall  
292 preservation and exposure of the interval, one section has been named the “type section”. The stratotype  
293 section for the K-Pg boundary is at El Kef, Tunisia (XXVIIIth International Geological Congress, 1989).  
294 The boundary itself has been linked to the anomalous abundance of Iridium that was derived from the  
295 impacting body.

296  
297 Close to the impact site reworked sedimentary deposits are mixed with ejecta from the impact. At  
298 intermediate distances the airborne ejecta may have arrived before the tsunamis; thus, airborne ejecta with  
299 higher Iridium concentrations may lie below rip up clasts and redeposited older sediments. In distant  
300 regions, high concentrations of Iridium used to define the K-Pg boundary (KieSSLing & Claeys, 2002) are  
301 thought to have arrived by settling from the stratosphere over a period up to several years (Claeys et al.,  
302 2002; Toon et al, 1982). This is compared to the modeled tsunami reaching a global extent in just two  
303 days. To verify the strength and pathway of the modeled impact tsunami we pay particular attention to  
304 these more distal regions (Schulte et al. 2010). In these regions the effects of the tsunami should be found  
305 in the interval immediately below the K-Pg boundary itself in both marine sections on land (supplementary  
306 table ST-1) and in scientific ocean drilling cores (supplementary table ST-2). We take any sign of missing  
307 biostratigraphic or paleomagnetic intervals or depositional disturbance immediately below this level (e.g.,  
308 erosional truncations of bedding or bioturbation features, sediment deformation, allochthonous clumps or  
309 clasts) as evidence of current activity or disturbance associated with the impact tsunami.

310  
311 A few of the studied boundary sections have paleomagnetic stratigraphy. The K-Pg boundary has been  
312 found to be within the upper half of subchron C29r in Gubbio, Italy (Lowrie and Alvarez, 1977) and  
313 Agost, Spain (Canudo et al., 1991). The estimated duration of the Cretaceous part of subchron C29r is 300  
314 kyr (Husson et al. 2011). Biostratigraphy often provides an important indication of missing section in  
315 deeper water, pelagic sections. The *Abathomphalus mayaroensis* Zone defines the uppermost Cretaceous  
316 foraminiferal zone in many of the older studies of the K-Pg boundary; however, Keller (1988) found that  
317 *A. mayaroensis* disappeared below the K-Pg boundary in the type section at El Kef. To fill this gap, Pardo

318 et al. (1996) defined a total range biozone (*Plummerita hantkeninoides*) that marks the top of the  
319 Maastrichtian and lies within the lower half of subchron C29r. The uppermost Cretaceous nannofossil  
320 zone is defined by the range of *Micula prinsii* (Sissingh, 1977). This Zone occupies most of the lower half  
321 of subchron C29r. Other fossil assemblages have been used to evaluate the ages within the Late  
322 Cretaceous, but they have not been well documented in more than one or two complete K-Pg boundary  
323 sections. Carbon and oxygen isotope stratigraphies have been generated for several of the K-Pg boundary  
324 sections (Supplementary Tables ST-1, ST-2). The records of the carbon isotopes show an abrupt break at  
325 the K-Pg boundary, with the isotopes becoming sharply negative (a drop of 2‰ at El Kef; Keller and  
326 Lindinger, 1989). However, the oxygen isotopes signal is more variable and may depend on what  
327 microfossils are being measured (c.f. El Kef, in Keller and Lindinger, 1989; MacLeod et al., 2018, and  
328 other sections in Caravaca, in Canudo et al., 1991; and in Zumaia, in Margolis et al., 1987).

329  
330 The advent of orbital tuning of geologic records has greatly advanced our ability to develop estimates of  
331 ages with comparable precision well back into the Cretaceous (e.g., Batenburg et al, 2012; Dinarés-Turrel  
332 et al., 2014; Husson et al., 2011 and references therein). These studies use calculated variations in the  
333 earth's orbit as a template for matching variations in stable isotopes, color, iron content, or bed thickness;  
334 however, beyond 60 Ma only the 405 kyr eccentricity cycle is known with sufficient accuracy to be used  
335 in tuning the time scale (Laskar et al., 2011; Westerhold et al., 2012). From these tuning efforts we know  
336 that the K-Pg boundary lies at the top of the 405 kyr orbital cycle of eccentricity designated as Ma405 1  
337 (Batenburg et al., 2012). Any effort at tuning must take place within a stratigraphic framework defined by  
338 other tools, normally a paleomagnetic stratigraphy, which in turn usually relies on a biostratigraphic  
339 framework.

340  
341 For the drill sites reported in this study, we list those sites (Supplementary Table ST-2) in which the K-Pg  
342 boundary interval is recovered and is fossiliferous, with stratigraphies that define the location of that  
343 boundary. Based on stratigraphic evaluations for both drilled cores and outcrop sections, we class the K-Pg  
344 boundary sections as: 1) complete, 2) apparently complete, 3) having a detectable depositional disturbance,  
345 hiatus, or disconformity, or 4) having a long erosional hiatus or non-depositional surface (Fig. 5). If such  
346 long missing sections range from the Cretaceous well up into the Paleocene or even younger sections, we  
347 cannot claim that they are attributable to the impact tsunami (category 4, above), and we discount them  
348 from our analysis. If, however, the lower part of the Paleocene is present, while a part of the Upper  
349 Cretaceous is missing, we classify this as possibly caused by the impact tsunami (category 3, above).

350

351 **4.2 Results**

352 The devastating effects of the asteroid impact in the Caribbean and Gulf of Mexico included earthquakes,  
353 slope failures, and debris flows, all of which could have contributed to tsunami formation, (e.g., Alegret  
354 and Thomas, 2005; Alvarez et al., 1992, 1995; Bourgeois et al., 1988; Bralower et al., 1998; Campbell et  
355 al., 2008; Denne et al., 2013, Keller et al., 1997, 2007; Kinsland et al., 2021; Maurrasse et al., 1991;  
356 Montanari et al., 1994; Schulte et al., 2006, 2008; Smit et al., 1996; Sanford et al., 2016; Stinnesbeck et  
357 al., 1997). These ancillary effects are not accounted for in the impact tsunami models, but nevertheless  
358 disrupted the K-Pg boundary. The modeled impact tsunami took principal radiation pathways directed to  
359 the east and northeast into the North Atlantic and to the southwest, through the Central American passage  
360 and into the southwestern Pacific (Fig. 4). At flow speeds greater than 20 cm/sec (Fig. 4b) the passing  
361 tsunami could have eroded fine-grained marine sediment even on the deep seafloor (Lonsdale and  
362 Southard, 1974; McCave, 1984).

363

364 The Tethys region, the South Atlantic, the North Pacific, and the Indian Ocean basins were largely  
365 shielded from the stronger effects of the tsunami (Fig. 4). This is consistent with the location of the  
366 several complete sections described from the marine outcrops around the Mediterranean, including the  
367 type section at El Kef (Fig. 5). It is also consistent with the frequent recovery of complete sections at  
368 scientific ocean drilling sites in the South Atlantic Ocean and on Seymour Island in the Antarctic  
369 Peninsula, the several complete sections of the K-Pg boundary recovered in the North Pacific Ocean and  
370 on the island of Hokkaido, and the complete K-Pg boundary intervals drilled on bathymetric highs in the  
371 eastern Indian Ocean.

372

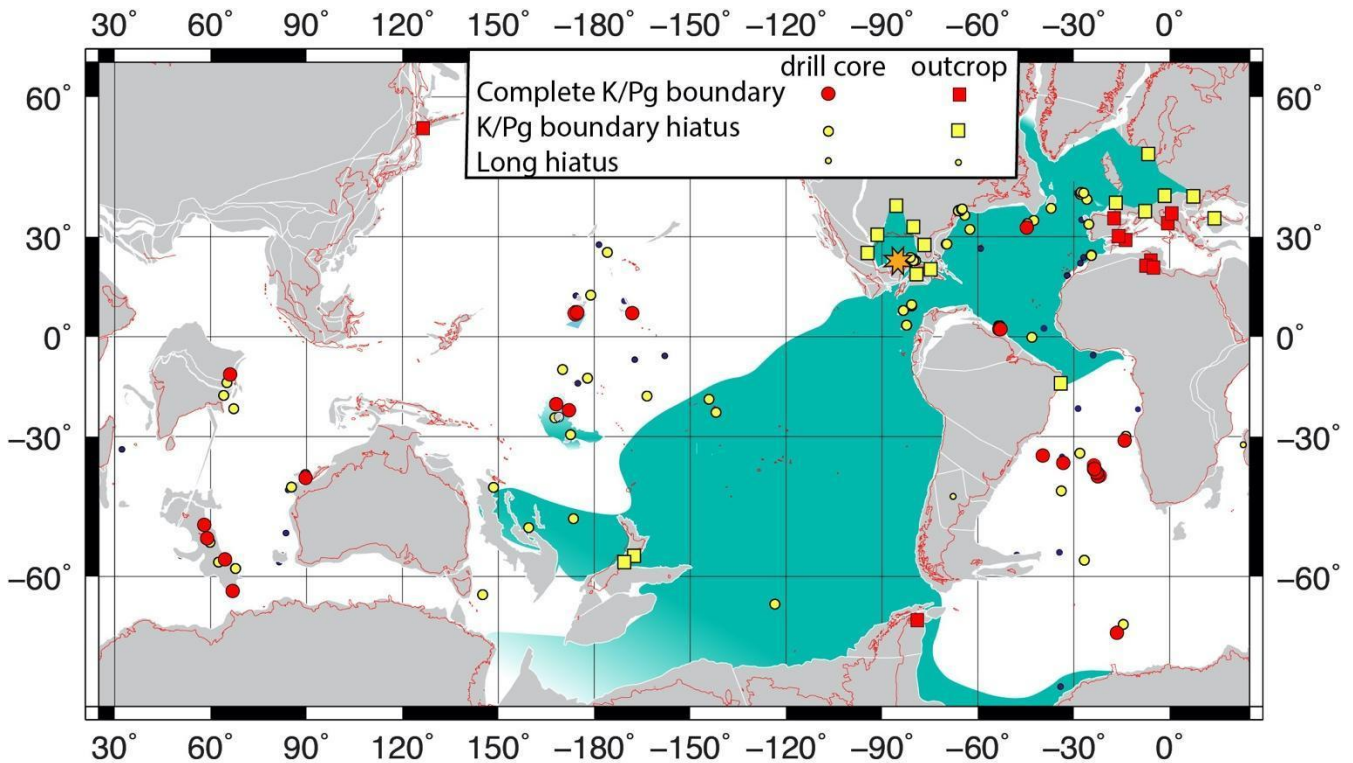
373 Looking at K-Pg boundary intervals that lay in the modeled pathway of the tsunami, the results of the  
374 comparison are also largely consistent. The drilled sections in New Jersey show gaps, rip up clasts, or  
375 tempestites in the K-Pg boundary interval. Sections studied in western Europe (Germany, Denmark,  
376 France, Bulgaria, Austria; Supplementary Table ST-1) generally show biostratigraphic gaps, erosional  
377 truncations, or slumps and gravity flows in the uppermost part of the Maastrichtian section. In the North  
378 Atlantic Ocean only three sites in two areas contain what appear to be complete K-Pg boundary intervals  
379 (Fig. 5). Site U1403 is the deepest site drilled on the J-Anomaly Ridge off Newfoundland. The Upper  
380 Cretaceous section is relatively thick here, lying between two southeast trending basement highs  
381 (Expedition 342 Scientists, 2012) and may represent a depocenter for sediment eroded from the nearby  
382 locations. Sites 1259 and 1260 are located on the slope of the Demerara Rise off Suriname, South  
383 America. During the Late Cretaceous their location was within a few degrees north of the equator and

384 may have been partially shielded from the main force of the tsunami (MacLeod et al., 2007). However,  
385 farther south on the coast near Recife, Brazil, at Pernambuco, a neritic section contains a graded sandy  
386 bed, including ejecta from the asteroid impact, and is overlain by an iridium anomaly (Albertaino and  
387 Martins, 1996).

388

389 Almost all the drill sites in the South Pacific basin appear to have a missing uppermost Maastrichtian  
390 section. This is true even on the southern part of the Ongtong-Java Plateau, which lies near the northern  
391 edge of higher velocities associated with the impact tsunami's modeled pathway, while two sites on the  
392 northern side of the Plateau (Sites 803 and 807) have the only complete K-Pg sections recovered in the  
393 South Pacific basin of 65 Ma (Figs. 4b, 5).

394



395

396 **Figure 5.** Plate reconstruction and site locations at 65 Ma from ODSN website  
397 (<http://www.odsn.de/odsn/services/paleomap/paleomap.html>) using the magnetic reference  
398 frame. Continental blocks in gray with modern continental outlines in red. Green shaded  
399 ocean areas depict approximate regions where the models of the K-Pg impact tsunami  
400 showed flow velocities in excess 20 cm/sec (see Fig. 4b). Most coastal regions were  
401 indicated by the models to have experienced such high velocities, but are not shown here.  
402 Drill site locations indicated by circles; K-Pg land outcrop sites indicated by squares (see  
403 legend). Small filled circles indicate sites with hiatuses of a million years or more duration  
404 that span the K-Pg boundary and range well into the Paleogene.

405



406 Of particular interest are the outcrops of the K-Pg boundary interval on the southeast corner of North  
407 Island and northeast corner of South Island, New Zealand. Here the olistostromal deposits at the top of the  
408 Upper Cretaceous Whangi Formation were originally explained as the result of local tectonic activity  
409 (Laird et al., 2003) or mass flow deposit (Hines et al., 2013); but considering the stratigraphic position of  
410 this deposit and its location directly in line with the modeled pathway of the impact tsunami, we feel the  
411 olistostrome is recording the effects of the impact tsunami (Figs. 4, 5, 6). Hollis (2003) reviewed 16  
412 marine sections in New Zealand that ranged in paleo water depth from inner shelf to upper bathyal and  
413 found that at least 14 of them probably had a missing or disturbed K-Pg boundary interval. However,  
414 detailed biostratigraphic control of the uppermost Maastrichtian is lacking for the remaining two sections,  
415 which raises the possibility that these sections may also be incomplete. Paleomagnetic control on the  
416 sections has not been obtained due to pervasive demagnetization (Kodama et al., 2007).

417

418 The tsunami models indicate that many coastal regions around the globe may have been affected by  
419 the impact tsunami; however, without a detailed knowledge of the bathymetry and coastal geometry at  
420 the end of the Cretaceous, and without a higher resolution model in these areas, we cannot evaluate  
421 how accurate the models might be in such shoreline areas. Our study shows that some distant near-  
422 shore areas were strongly affected (e.g., New Jersey, New Zealand, Pernambuco), while others were  
423 not (e.g., Seymour Island, Hokkaido). Still, it is probably significant that the models show only minor  
424 coastal effects in the shielded Tethys basin (Fig. 5, 6) where all the neritic sections appear to be  
425 complete (Supplementary Table ST-1).

426

427 In a similar manner, all the large, relatively shallow oceanic plateaus and rises show up in the higher  
428 velocity regions of the models (Fig. 4b); however, as in the coastal regions, the resolution of the models  
429 and that of the paleo bathymetry do not allow detailed comparison of the model results with the  
430 completeness of the recovered sections. We feel it is significant that only those prominent bathymetric  
431 highs that lie outside the main pathway of the impact tsunami show a preponderance of complete K-Pg  
432 sections (Figs 4b, 5).

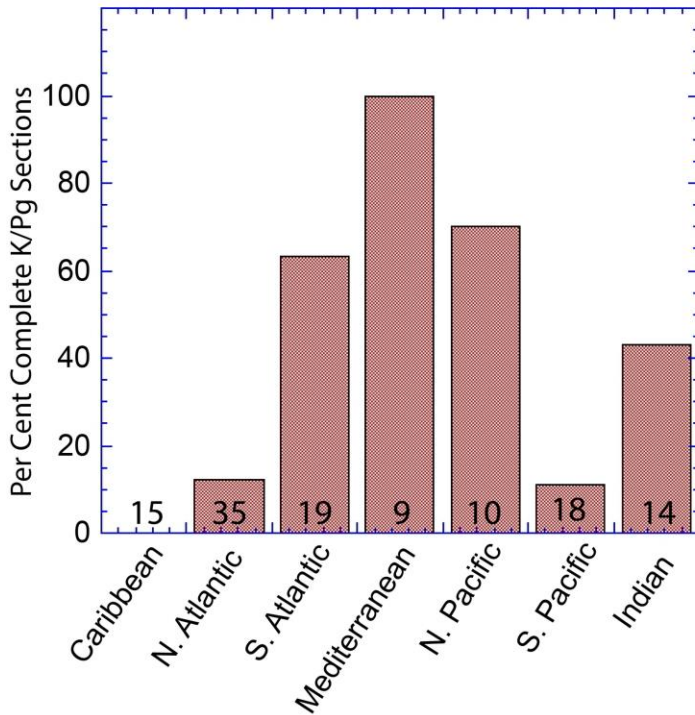


**Figure 6.** The percent of apparently complete marine sections containing the K-Pg boundary interval listed by ocean basin, including both marine sections found on the surrounding land and in scientific ocean drilling cores. Data do not include sites with long hiatuses (see text). The number of sections studied is shown at the base of each column (see Supplementary Tables ST-1 and ST-2). No complete sections were found in the Caribbean (including the Gulf of Mexico). The South Atlantic and South Pacific categories include sites studied in the Southern Ocean sector of these basins.

452 A summary of the studied marine sections on land and in drill cores is shown in Figure 6. As noted above,  
 453 all marine sections on land around the Mediterranean lie outside the modeled >20 cm/sec flow velocity  
 454 contour (Fig. 4b, 5) and are believed to have complete K-Pg boundary records. Also noted above, the  
 455 Caribbean-Gulf of Mexico region lies within the area of very high flow velocities and have no complete,  
 456 undisturbed sections. Similarly, the North Atlantic Basin is an area of high flow velocities and has only  
 457 four sites (11% of sites studied) that are apparently complete (ST-1, ST-2). The South Pacific region with  
 458 flow velocities > 20 cm/sec (Figs. 4b, 5) have two sites (11% of sites studied) that appear to be complete.  
 459

460 At least 65% of the studied sections in regions where modeled flow velocities are <20 cm/sec have  
 461 complete sections. In regions with flow velocities >20 cm/sec, 91% of the studied sections have  
 462 incomplete K-Pg boundary sections. The most telling confirmation of the global significance of the  
 463 impact tsunami is the highly disturbed and incomplete sections on the eastern shores of North and South  
 464 Islands of New Zealand. These sites lie directly in the path of the tsunami propagation, more than 12,000  
 465 km distant from the impact location (Figs. 4, 5).

466

467

468

469

## 470 **5 Discussion**

### 471 **5.1 Tsunami Mechanisms**

472 Earlier theoretical and regional simulations (e.g., Ward, 2012; Matsui et al., 2002; Wünnemann and Weiss,  
473 2015) differ on whether the rim wave or collapse wave dominates with respect to energy. The rim wave  
474 refers to the water displaced from the impact that is pushed away from the origin (Wünnemann and Weiss,  
475 2015). The collapse wave is the secondary process arising from the cavity collapse in the crater and water  
476 rushing into the crater (Wünnemann and Weiss, 2015). To test the relative contributions of the collapse  
477 and rim waves to the total tsunami energy, we ran a simulation ('Crater Only') with no rim wave or  
478 velocity, such that the tsunami is solely due to the collapse wave filling in the crater. Our results agree  
479 with the conclusion of Wünnemann and Weiss (2015), that the rim wave is the source of most of the  
480 energy for this impact tsunami. Four hours after impact, the 'Crater Only' case is about 13 times less  
481 energetic than the 'Full Crater, With Rim Wave' case. The MOM and MOST model simulations of the  
482 Full Crater scenario showed similar energy numbers four hours post-handoff ( $3.9 \times 10^{19}$  and  $3.84 \times 10^{19}$  J  
483 correspondingly), such that the model energy estimates appear to be robust and independent of the exact  
484 model used.

485 The efficiency of tsunamis can be quantified by the ratio between tsunami energy and the source energy.  
486 The efficiency of tsunami generation by the Chicxulub impact is similar to that of large earthquakes. The  
487 energy ratio for earthquake-generating tsunamis averages around 0.1% (with large variations from 0.02%  
488 to 0.8%, Tang et al., 2012), while we predict that the Chicxulub tsunami has an efficiency of 0.19% (SI  
489 Table 4). SI Figure 4 shows that the impact tsunami energy dissipates relatively quickly, relative to  
490 seismogenic tsunamis, consistent with the "Van Dorn effect" (Van Dorn et al., 1968) of faster wave energy  
491 attenuation due to large non-linearities near the source of explosion-generated tsunamis. Near-field  
492 tectonic activity, triggered by passage of strong stress wave produced by the impact, was not included in  
493 our simulations. It is likely that any earthquake generated slides and collapses would be minor relative to  
494 the primary rim wave.

495

### 496 **5.2 Hiatus Distribution**

497 The better preserved, thicker, carbonate-rich sections in the oceans are commonly found on bathymetric  
498 highs such as continental terraces, oceanic plateaus, rises, aseismic ridges, and seamounts. Drill sites in  
499 which the K-Pg boundary is clearly identified are usually found in such locations. These locations do have  
500 their own problems, however. Such regions of bathymetric prominence also give rise to enhanced

501 turbulence in the waters surrounding them (Cacchione & Drake, 1986; Cacchione et al., 2002; Rudnick et  
502 al., 2003; Wunsch & Ferrari, 2004); thus, they enhance the erosional power of tsunamis and tidal waves  
503 that pass over them. The preserved sedimentary sections atop bathymetric highs usually show clear  
504 evidence of erosion and the sculpting of pelagic deposits that sit upon them. The drilling strategy often  
505 employed by scientific ocean drilling expeditions takes advantage of the stratigraphic character of these  
506 deposits to sample relatively older intervals where overburden has been removed or was never deposited,  
507 the intention being to minimize the effects of diagenetic alteration on these older sediments. At other sites,  
508 full advantage was taken of the thicker, more complete sections to study the detailed paleoceanographic  
509 history. This duality of purpose means that many sites drilled on bathymetric highs contain significant  
510 gaps in the stratigraphic record, while on some highs there are close-by sites that have recovered complete  
511 sections. In regions with modeled flow velocities  $< 20$  cm/sec, several sites locate the K-Pg boundary  
512 between recovered cores (ST-2); thus, the amount of missing section (if any) and the exact nature of the  
513 boundary is uncertain.

514

515 In basins where almost all sites show incomplete uppermost Maastrichtian sections there are still a few  
516 deep-sea sections that appear to be complete (e.g., Sites 1259, 1260, U1403 in the North Atlantic). These  
517 may represent local bathymetric shielding from erosion or local depocenters that receive sediment which  
518 has been eroded from nearby areas. The coincidence of regions having few if any complete K-Pg boundary  
519 sections and the pathway of relatively strong tsunami flow, combined with the more common occurrence  
520 of complete K-Pg boundary sections in regions that did not have strong tsunami flow, support the results  
521 of the tsunami models. The lack of complete K-Pg boundary sections in the southern South Pacific and on  
522 the eastern shores of New Zealand strongly suggest that this tsunami was of global significance, reaching  
523 at least 12,000 km across the deep ocean. It also suggests that except for some shallow coastal regions,  
524 areas such as the Tethyan region, the North Pacific, the South Atlantic and much of the Indian Ocean basin  
525 were largely geographically shielded from the effects of the tsunami

526

### 527 **5.3 Comparison with Large Historical Tsunamis**

528 To provide perspective on the size of the impact tsunami, we compare our impact tsunami model estimates  
529 with some representative large historical tsunamis. The 2004 Indian Ocean tsunami (Smith et al., 2005) is  
530 possibly the largest modern-era tsunami; it killed over 230,000 people around the Indian Ocean and was  
531 recorded around the globe (Titov et al., 2005). The 2011 Tohoku tsunami was generated by a similarly  
532 strong earthquake and has become the costliest natural disaster of all time. Offshore amplitudes of the

533 2004 Indian Ocean tsunami 2 hours after generation were measured to be about 0.6 m, and 2 meter waves  
534 were measured about 500 km away from the epicenter of the 2011 Tohoku tsunami, at a seafloor depth of  
535 5700 m. These deep-ocean amplitudes led to runup at coastlines of up to 40 m (Sumatra Island) and 50 m  
536 (Honshu Island). The 1883 Krakatau event generated another catastrophic tsunami with explosive-type  
537 initial conditions, potentially similar to the impact generation. The Krakatau wave devastated local  
538 coastlines, killing over 30,000 (second most deadly record after the Indian Ocean tsunami) with waves that  
539 ran up to 40 m and traveled distances of up to 5 km inland, but did not generate significant waves outside  
540 Sunda Strait. All these tsunamis, among the largest in recorded history, are dwarfed by the wave  
541 amplitudes and energy of the simulated Chicxulub tsunami. The Chicxulub tsunami produces offshore  
542 amplitudes over 1 m around most of the world oceans (Figure 4a). When tsunamis reach the shallow  
543 waters of a coastline or bathymetric high, wave amplitude increases due to shoaling. Comparison of our  
544 tsunami simulations with observations and modeling of the strongest recent tsunamis of 2004 and 2011  
545 implies that the coastal amplitudes for the Chicxulub tsunami would flood most coastlines, in a manner  
546 that would be catastrophic in modern times. The total energy of our impact tsunami simulations is  
547 compared with the energy of these large historical tsunamis in SI Table 4 and SI Figure 4. Energy values  
548 are calculated according to standard formulae for shallow-water energy (e.g., Arbic et al., 2004; their  
549 equation 14). SI Figure 4 displays the ratios of energy in the impact tsunami simulations to the 2004  
550 Indian Ocean tsunami, as a function of time into the ocean simulation. The energy in the impact tsunami  
551 decays faster than the energy in the 2004 Indian Ocean tsunami – another manifestation of the “Van Dorn  
552 effect”. The initial energy in the impact tsunami was up to 30,000 times larger than the energy of any  
553 historically documented tsunamis. Wave energies in the ‘Half Crater’ simulation are about 5% less than  
554 those in the ‘Full Crater’ simulation. The ‘Crater Only’ simulation, without the large rim wave, still has  
555 much more energy than any other historical tsunamis. For a wide variety of sources, the portion of the  
556 source energy that goes into tsunami generation is less than 1%, with large variations from about 0.01% to  
557 0.3% (SI Table 4). An impact- and explosion-type of tsunami generation appears to have similar efficiency  
558 in transferring energy into long wave propagation. However, impact- and explosion-generated tsunamis  
559 dissipate energy much faster during propagation. Nevertheless, the sheer amount of energy of the impactor  
560 is sufficient to generate a giant global tsunami, even if only 0.2% of the impact energy goes into the  
561 tsunami.

562

#### 563 **5.4 Future work**

564 The first global simulation of the Chicxulub impact tsunami demonstrates that it was much larger than any  
565 recent earthquake-generated tsunami, and that it was likely large enough to leave a mark on marine

566 sediment records. Many uncertainties remain, and there is much room for improvement in future  
567 studies. It is well known that most impacts are oblique with 45° impact angle being most likely (e.g.,  
568 Robertson et al., 2021). With sufficient computer power, high-resolution, three-dimensional hydrocode  
569 simulations of the first ten or so minutes could be performed, thus allowing for varying water depth, non-  
570 perpendicular impact angles, and other key uncertainties in the hydrocode simulation. Generally, we would  
571 expect a slightly larger rim wave in the downrange direction and a smaller wave up range. It may be  
572 instructive to vary initial conditions of the global simulation in a parameterized way to crudely account for  
573 impact angle.

574

575 The January 15, 2022, Hunga Tonga-Hunga Ha'apai volcano explosion has demonstrated an additional  
576 mechanism of tsunami generation from large explosive events – the low frequency air pressure wave, e.g.  
577 Lamb wave (Duncombe, 2022). While the exact mechanism of the air pressure Lamb wave is not fully  
578 understood, it is clear that significant waves can be generated from such air pressure waves propagating  
579 over oceans. The full analysis of such tsunami generation is out of the scope of this paper and is a subject  
580 of future research. But based upon observations and initial modeling of the Tonga event, it is clear that the  
581 Lamb wave can be a source of significant secondary tsunamis around the world. These waves would reach  
582 world coastlines much earlier than the tsunami generated by the crater formation. The energy of the  
583 Chicxulub impact is at least 100,000 times larger than the Tonga explosion. The Lamb wave from the  
584 Tonga explosion generated tsunami waves of over a meter at some locations around the Pacific and up to  
585 half a meter at other oceans. Thus, the Lamb wave from the Chicxulub explosion can be a significant  
586 source of tsunamis in the far-field from the impact source, and will be a subject of future work.

587

588

## 589 **Acknowledgments, Samples, and Data**

590 **Supplementary Information** is linked to the online version of the paper.

591

592 **Acknowledgments:** We thank Gareth Collins, Finn Løvholt, Clemens Rumpf, and two anonymous  
593 reviewers for comments and suggestions that led to significant improvements in the manuscript. B.K.A.  
594 thanks Sarah Stamps for useful conversations. M.M.R. and B.K.A. thank Mark Champe, Charles  
595 Antonelli, and Michael Messina for help with setting up MOM6 on University of Michigan  
596 computers. M.M.R., B.K.A., and J.K.A. acknowledge funding support from US National Science  
597 Foundation grants OCE-0968783 and OCE-1351837, a Research Experience for Undergraduates (REU)  
598 supplement for MMR to OCE-1351837, and the University of Michigan Associate Professor Support Fund  
599 supported by the Margaret and Herman Sokol Faculty Awards. We gratefully acknowledge the developers  
600 of iSALE-2D, including Gareth Collins, Kai Wünnemann, Dirk Elbeshausen, Tom Davison, Boris Ivanov

601 and Jay Melosh. Some plots in this work were created with the pySALEPlot tool written by Tom Davison.  
602 The MOM6 simulations in this paper were carried out on the Flux supercomputer provided by the  
603 University of Michigan Advanced Research Computing Technical Services. Much of B.K.A.'s  
604 contributions to this paper took place while he was on sabbatical in France. B.K.A. thanks many French  
605 colleagues, especially Thierry Penduff, Rosemary Morrow, Nadia Ayoub, and Florent Lyard, for their help  
606 in procuring this sabbatical year. He Wang's contributions from GFDL are supported by NOAA's Science  
607 Collaboration Program and administered by UCAR's CPAESS under awards NA16NWS4620043 and  
608 NA18NWS4620043B. This is contribution number 5300 of NOAA-PMEL. Results, bathymetry, and  
609 initial conditions of our work can be found at  
610 <https://dataverse.harvard.edu/dataset.xhtml?persistentId=doi:10.7910/DVN/GWOFIO&version=DRAFT>.  
611 This is a draft repository; upon acceptance a permanent doi and link will be provided.

612  
613 **Author Contributions:** M.M.R. converted the hydrocode results into the initial conditions for the MOM6  
614 tsunami simulations, ran the MOM6 simulations, and wrote the paper. B.K.A. oversaw the project. B.C.J.  
615 ran the iSALE hydrocode simulations and greatly contributed to the design of the final simulations.  
616 T.C.M. conceived the project in a conversation with B.K.A. Together with C.J.H. he provided geologic  
617 information on the studied K-Pg sections. V.T. ran the MOST simulations and guided comparisons of  
618 MOST and MOM6 results. A.J.A., J.K.A., and H.W. helped M.M.R. set up and run the MOM6 model on  
619 University of Michigan computers. J.K.A. also helped M.M.R. to construct initial conditions. J.R.  
620 initiated discussions that greatly improved our initial conditions and eventually led to the use of iSALE.  
621 C.R.S. provided the bathymetry for the K/Pg Boundary. All authors contributed to improving the  
622 manuscript.

623  
624 The authors declare no conflict of interest.

625  
626

## 627 **References**

- 628 Adcroft, A. (2013). Representation of topography by porous barriers and objective interpolation of  
629 topographic data. *Ocean Modelling*, 67, 13-27, <https://doi.org/10.1016/j.ocemod.2013.03.002>.
- 630  
631 Adcroft, A. (2017). NOAA - GFDL MOM6 Examples, *Github*. Available from:  
632 <https://github.com/NOAA-GFDL/MOM6-examples/wiki>
- 633  
634 Albertao, G.A., & Martins Jr., P.P. (1996). A possible tsunami deposit at the Cretaceous-Tertiary  
635 boundary in Pernambuco, northeastern Brazil. *Sedimentary Geology*, 104, 189-201.
- 636  
637 Alegret, L. & Thomas, E., (2005). Cretaceous/Paleogene boundary bathyal paleo-environment in the  
638 central North Pacific (DSDP Site 465), the Northwestern Atlantic (ODP Site 1049), the Gulf of  
639 Mexico and the Tethys: The benthic foraminiferal record. *Earth and Planetary Science Letters*,  
640 224, 53-82
- 641  
642 Alvarez, W., Smit, J., Lowrie, W., Asaro, F., Margolis, S.V., Claeys, P., Kastner, M., & Hildebrand, A.R.  
643 (1992). Proximal impact deposits at the Cretaceous-Tertiary boundary in the Gulf of Mexico: A  
644 restudy of DSDP Leg 77 Sites 536 and 540. *Geology*, 20, 697-700.
- 645  
646 Alvarez, W., Claeys, P., & Kieffer, S.W. (1995). Emplacement of Cretaceous-Tertiary boundary shocked  
647 quartz from Chicxulub Crater. *Science*, 269, 930-935.

648

649 Anderson, J.L.B., Schultz, P.H., & Heineck, J.T. (2003). Asymmetry of ejecta flow during oblique impacts  
650 using three-dimensional particle image velocimetry. *Journal of Geophysical Research: Planets*, 108,  
651 5094, <https://doi.org/10.1029/2003JE002075>.

652 Arbic, B.K., Garner, S.T., Hallberg, R.W., & Simmons, H.L. (2004). The accuracy of surface elevations  
653 in forward global barotropic and baroclinic tide models. *Deep-Sea Research II*, 51, 3069-3101,  
654 <https://doi.org/10.1016/j.dsr2.2004.09.014>.

655 Bardeen, C.G., Garcia, R.R., Toon, O.B., & Conley, A.J. (2017). On transient climate change at the  
656 Cretaceous-Paleogene boundary due to atmospheric soot injections. *Proceedings of the National*  
657 *Academy of Sciences of the United States of America*, 114(36), E7415–E7424.  
658 <https://doi.org/10.1073/pnas.1708980114>.

659 Bahlburg, H., Weiss, R., & Wünnemann, K. (2010). Low energy deposition in the Chicxulub crater during  
660 the impact to post-impact transition. *Earth and Planetary Science Letters*, 295, 170–176,  
661 <https://doi.org/10.1016/j.epsl.2010.03.037>.

662 Batenburg, S.J., Sprovieri, M., Gale, A.S., Hilgen, F.J., , Hüsing, S., Laskar, J., Liebrand, D, Lirer, F.,  
663 Orue-Etxebarria, X., Pelosi, N., & Smit, J. (2012). Cyclostratigraphy and astronomical tuning of  
664 the Late Maastrichtian at Zumaia (Basque country), Northern Spain. *Earth and Planetary Science*  
665 *Letters*, 359-360, 264-278, <https://doi.org/10.1016/j.epsl.2012.09.054>

666 Bell, C., Morgan, J.V., Hampson, G.J., & Trudgill, B. (2004). Stratigraphic and sedimentological  
667 observations from seismic data across the Chicxulub impact basin. *Meteoritics & Planetary Science*,  
668 39(7), 1089–1098. <https://doi.org/10.1111/j.1945-5100.2004.tb01130.x>.

669 Bourgeois, J., Hansen, T.A., Wiberg, P.L. & Kauffman, E.G. (1988). A tsunami deposit at the  
670 Cretaceous-Tertiary boundary in Texas. *Science*, 241, 567–570.

671 Bralower, T.J., & Paull, C.K. (1998) The Cretaceous-Tertiary boundary cocktail: Chicxulub impact  
672 triggers margin collapse and extensive sediment gravity flow, *Geology*, 26(4), 331-334.

673 Brugger, J., Feulner, G., & Petri, S. (2017). Baby, it's cold outside: Climate model simulations of the  
674 effects of the asteroid impact at the end of the Cretaceous. *Geophysical Research Letters*, 44(1), 419–  
675 427, <https://doi.org/10.1002/2016GL072241>

676 Burwell, D., Tolkova, E., & Chawla, A. (2007). Diffusion and dispersion characterization of a numerical  
677 tsunami model. *Ocean Modelling*, 19, 10–30, <https://doi.org/10.1016/j.ocemod.2007.05.003>

678 Busby, C.J., Yip, G., Blikra, L., & Renne, P. (2002). Coastal landsliding and catastrophic sedimentation  
679 triggered by Cretaceous-Tertiary bolide impact: A Pacific margin example? *Geology*, 30(8), 687–690,  
680 [https://doi.org/10.1130/0091-7613\(2002\)030<0687:CLACST>2.0.CO;2](https://doi.org/10.1130/0091-7613(2002)030<0687:CLACST>2.0.CO;2)

681 Cacchione, D.A. & Drake, D. E. (1986), Nepheloid Layers and Internal Waves Over Continental Shelves  
682 and Slopes, *Geo-Marine Letters*, 6, 147-152.

683 Cacchione, D. A., Pratson, L. F. & Ogston, A. S. (2002), The shaping of continental slopes by internal  
684 tides, *Science*, 29, 724-727



- 685 Campbell, C.E., Oboh-Ikuenobe, F.E., Eifert, E.I. (2008). Mega tsunami deposit in Cretaceous-  
686 Paleogene boundary interval of southeastern Missouri. *Geological Society of America Special*  
687 *Paper* 437, 189-198.
- 688 Canudo, J.I., Keller, G., & Molina, E. (1991). Cretaceous/Tertiary boundary extinction pattern and  
689 faunal turnover at Agost and Caravaca, S.E. Spain. *Marine Micropaleontology*, 17, 319-341.  
690 [https://doi.org/10.1016/0377-8398\(91\)90019-3](https://doi.org/10.1016/0377-8398(91)90019-3)
- 691 Claeys, P., Kiessling, W., & Alvarez, W. (2002). Distribution of the ejecta at the Cretaceous- 607Tertiary  
692 boundary, In C. Koeberl & K. G. MacLeod, (Eds.) Catastrophic events and mass 608  
693 extinction: impacts and beyond. *Geological Society of America Special Paper* 356, 55–69. 609
- 694 Collins, G.C., Melosh, H.J., & Ivanov, B.A. (2004). Modeling damage and deformation in numerical  
695 impact simulations. *Meteoritics and Planetary Science*, 39(2), 217–231, [https://doi.org/10.1111/j.1945-](https://doi.org/10.1111/j.1945-5100.2004.tb00337.x)  
696 [5100.2004.tb00337.x](https://doi.org/10.1111/j.1945-5100.2004.tb00337.x)
- 697 Collins, G.S., Patel, N., Davison, T.M., Rae, A.S. P., Morgan, J.V., Gulick, S.P S., et al. (2020) A steeply-  
698 inclined trajectory for the Chicxulub impact. *Nature Communications* 11, 1480.  
699 <https://doi.org/10.1038/s41467-020-15269-x>.
- 700 Collins, G.S., Morgan, J., Barton, P., Christeson, G.L., Gulick, S., Urrutia, J., Warner, M., & Wünnemann,  
701 K. (2008). Dynamic modeling suggests terrace zone asymmetry in the Chicxulub crater is caused by  
702 target heterogeneity. *Earth and Planetary Science Letters*. <https://doi.org/10.1016/j.epsl.2008.03.032>
- 703 Denne, R.A. , Scott, E.D., Eickhoff, D.P., Kaiser, J.S., Hill, R.J., & Spaw, J.M. (2013). Massive  
704 Cretaceous-Paleogene boundary deposit, deep-water Gulf of Mexico: New evidence for widespread  
705 Chicxulub-induced slope failure: *Geology*, 42(9), 983-986, <https://doi.org/10.1130/G34503.1>
- 706 Dinarès-Turella, J., Westerhold, T., Pujalte, V., Röhl, U., & Kroon, D. (2014). Astronomical calibration of  
707 the Danian stage (Early Paleocene) revisited: settling chronologies of sedimentary records across the  
708 Atlantic and Pacific Oceans: *Earth and Planetary Science Letters*, 405, 119–131.
- 709 Duncombe, J. (2022). The surprising reach of Tonga’s giant atmospheric waves. *Eos*,  
710 103, <https://doi.org/10.1029/2022EO220050>. Published on 21 January 2022.
- 711 Expedition 342 Scientists. (2012). Paleogene Newfoundland sediment drifts. *Integrated Ocean Drilling*  
712 *Program, Preliminary Report, 342*. <https://doi.org/10.2204/iodp.pr.342.2012>
- 713 Gisler, G., Weaver, R., & Gittings, M. (2011). Calculations of asteroid impacts into deep and shallow  
714 water. *Pure and Applied Geophysics*, 168, 1187-1198, <https://doi.org/10.1007/s00024-010-0225-7>
- 715 Glimsdal, S., Pedersen, G.K., Langtangen, H.P., Shuvalov, V., and Dypvik, H. (2007). Tsunami generation  
716 and propagation from the Mjølnir asteroid impact. *Meteoritics & Planetary Science*, 42, 1473-1493.  
717 <https://doi.org/10.1111/j.1945-5100.2007.tb00586.x>
- 718 Gulick, S.P.S., Barton, P.J., Christeson, G.L., Morgan, J.V., McDonald, M., Mendoza-Cervantes,  
719 K., Pearson, Z.F., Surendra, A., Urrita-Fucugauchi, J., Vermeesch, P.M., & Warner, M.R. (2008).  
720 Importance of pre-impact crustal structure for the asymmetry of the Chicxulub impact crater. *Nature*  
721 *Geoscience*, 1, 131-135, <https://doi.org/10.1038/ngeo103>

- 722 Gulick, S., Morgan, J., and Mellett, C.L. (2016). *Expedition 364 Scientific Prospectus: Chicxulub: drilling*  
723 *the K-Pg impact crater*. International Ocean Discovery Program.  
724 <https://doi.org/10.14379/iodp.sp.364.2016>
- 725 Hines, B.R., Kulhanek, B.K., Hollis, C.J., Atkins, C.B., & H E G Morgans, H.E.G., (2013). Paleocene–  
726 Eocene Stratigraphy and Paleoenvironment at Tora, Southeast Wairarapa, New Zealand, New Zealand  
727 Journal of Geology and Geophysics, <https://doi.org/10.1080/00288306.2013.836112>
- 728 Hollis, C. J. (2003). The Cretaceous/Tertiary boundary event in New Zealand: profiling mass extinction.  
729 *New Zealand: Journal of Geology and Geophysics*, 46, 307-321.
- 730 Husson, D., GalbrunB., Laskar , J., Hinnov, I.A., Thibault, N., Gardin, S., and Locklair, R.E. (2011).  
731 Astronomical calibration of the Maastrichtian (Late Cretaceous): *Earth and Planetary Science Letters*,  
732 128, 128-340.
- 733 International Geologic Congress, (1989). 28th International Geological Congress, Washington, D.C, July  
734 9- 19,624 p., doi 10.1016/0045-8732(88)90022-1
- 735 Keller, G. (1988). Extinction, survivorship and evolution of planktic foraminifers across the  
736 Cretaceous/Tertiary boundary at El Kef, Tunisia. *Marine Micropaleontology*, 13, 239-263.
- 737 Keller, G., & Lindinger, M. (1989). Stable isotope, TOC and CaCO<sub>3</sub> record across the Cretaceous/Tertiary  
738 boundary at El Kef, Tunisia. *Palaeogeography, Palaeoclimatology, Palaeoecology*, 73, 243-265.
- 739 Keller, G., Lopez-Oliva, J.G., Stinnesbeck, W., & Adatte, T. (1997). Age, stratigraphy, and deposition of  
740 near-K/T siliciclastic deposits in Mexico: Relation to bolide impact. *Geological Society of America*  
741 *Bulletin*, 109, 410–428.
- 742 Keller, G., Adatte, T., Berner, Z., Harting, M., Baum, G., Prauss, M., Tantawy, A., & Stueben, D. (2007).  
743 Chicxulub impact predates K–T boundary: New evidence from Brazos, Texas. *Earth and Planetary*  
744 *Science Letters*, 255, 339-356.
- 745 Kiessling, W., & Claeys, P. (2001). A geographic database approach to the KT boundary, In E. Buffetaut  
746 & C. Koeberl (Eds.) *Geological and biological effects of impact events*. (Berlin, Springer), 83–140.
- 747 Kinsland, G.L., Egedahl, K., Strong, M.A., & Ivy, R. (2021). Chicxulub impact tsunami megariipples in  
748 the subsurface of Louisiana: Imaged in petroleum industry seismic data. *Earth and Planetary Science*  
749 *Letters*, 570, 007063, <https://doi.org/10.1016/j.epsl.2021.117063>
- 750 Kodama, K., Fukuoka, M., Aita, Y., Sakai, T., Hori, R.S., Takemura, A., Campbell, H.J., Hollis, C.J.,  
751 Grant-Mackie, J.A., and Spörli, K.B., 2007, Paleomagnetic results from Arrow Rocks in the  
752 framework of paleomagnetism in pre-Neogene rocks from New Zealand, in Spörli, in K.B., Takemura,  
753 A., and Hori, R.S., (Eds.) The Oceanic Permian/Triassic Boundary Sequence at Arrow Rocks  
754 (Oruatemanu), Northland, New Zealand: Lower Hutt, New Zealand, *Geological and Nuclear Science*  
755 *Monograph* 24, 177–196.
- 756 Kunkel, C.M., Hallberg, R.W., & Oppenheimer, M. (2006). Coral reefs reduce tsunami impact in model  
757 simulations, *Geophysical Research Letters* 33, L23612, <https://doi.org/10.1029/2006GL027892>.

- 758 Laird, M.G., Bassett, K. N., Schiøler, P., Morgans, H. E. G, Bradshaw, J. D. & Weaver, S.D. (2003).  
759 Paleoenvironmental and tectonic changes across the Cretaceous/Tertiary boundary at Tora, southeast  
760 Wairarapa, New Zealand: A link between Marlborough and Hawke's Bay. *New Zealand Journal*  
761 *of Geology and Geophysical*, 46, 275-293.
- 762 Laskar, J., Fienga, A., Gastineau, M., and Manche, H. (2011). La2010: a new orbital solution for the long-  
763 term motion of the Earth. *Astronomy and Astrophysics*, 532, A89. [http://dx.doi.org/10.1051/0004-](http://dx.doi.org/10.1051/0004-6361/201116836)  
764 [6361/201116836](http://dx.doi.org/10.1051/0004-6361/201116836).
- 765 Lonsdale, P., & Southard, J. B. (1974). Experimental erosion of north pacific red clay: *Marine Geology*,  
766 17, M51– M60.
- 767 Lowrie, W., & Alvarez, W. (1977). Upper Cretaceous-Paleocene magnetic stratigraphy at Gubbio, Italy.  
768 III. Upper Cretaceous magnetic stratigraphy. *Geological Society of America Bulletin*, 88, 374-377.
- 769 MacLeod, K.G., Whitney, D.L., Huber, B. T., & Koeberl, C. (2007). Impact and extinction in remarkably  
770 complete Cretaceous-Tertiary boundary sections from Demerara Rise, tropical western North Atlantic.  
771 *Geological Society of America Bulletin*, v.119 (1/2), 101–115;. doi:10.1130/B25955.1.
- 772 MacLeod, K.G., Quinton, P.C., Sepúlveda, J. & Negra, M.H. (2018). Postimpact earliest Paleogene  
773 warming shown by fish debris oxygen isotopes (El Kef, Tunisia). *Science*, 360, 1467–1469.
- 774 Margolis, S.V., Mount, J.F. & Doehne, E. (1987). The Cretaceous/Tertiary boundary carbon and oxygen  
775 isotope stratigraphy, diagenesis, and paleoceanography at Zumaya, Spain: *Paleoceanography*, 2 (4),  
776 361-377.
- 777 Matsui, T., Imamura, F., Tajika, E., Nakano, Y., & Fujisawa, Y. (2002). Generation and propagation of a  
778 tsunami from the Cretaceous-Tertiary impact event. *Catastrophic Events and Mass Extinctions:*  
779 *Impacts and Beyond*, (356), 69–77. <https://doi.org/10.1130/0-8137-2356-6.69>.
- 780 Maurrasse, F. J.-M. R., and Sen, G. (1991). Impacts, tsunamis and the Haitian Cretaceous-Tertiary  
781 boundary layer. *Science*, 252, 1690–1693.  
782
- 783 McCave, I.N. (1984). Erosion, transport and deposition of fine-grained marine sediments. *Fine-Grained*  
784 *Sediments; Deep-Water Processes and Facies*, 15(1), 35–69.  
785 <https://doi.org/10.1144/GSL.SP.1984.015.01.03>
- 786 Montanari, A., Claeys, P., Asaro, F., Bermudez, J., & Smit, J. (1994). Preliminary stratigraphy and iridium  
787 and other geochemical anomalies across the KT boundary in the Bochil Section (Chiapas, southeastern  
788 Mexico), in New developments regarding the K/T event and other catastrophes in Earth history. *Lunar*  
789 *and Planetary Institute Contribution* 825, 84–85.
- 790 Morgan, J., Artemieva, N., & Goldin, T. (2013). Revisiting wildfires at the K-Pg boundary. *Journal of*  
791 *Geophysical Research: Biogeosciences*, 118(4), 1508–1520. <https://doi.org/10.1002/2013JG002428>
- 792 Morgan, J.V, Gulick, S.P.S., Bralower, T., Chenot, E., Christeson, G., Claeys, P., et al. (2016). The  
793 formation of peak rings in large impact craters. *Science*, 354(6314), 878–882,  
794 <https://doi.org/10.1126/science.aah6561>

- 795 Müller, R.D., Sdrolias, M., Gaina, C., Steinberger, B., & Heine, C. (2008). Long-term sea-level  
796 fluctuations driven by ocean basin dynamics. *Science* 319, 1357-1362,  
797 <https://doi.org/10.1126/science.1151540>.
- 798 Pardo, A., Ortiz, N. & Keller, G. (1996). Latest Maastrichtian foraminiferal turnover and its  
799 environmental implications at Agost, Spain. In: In N. Macleod & G. Keller (Eds.), *The*  
800 *Cretaceous/Tertiary Boundary Mass Extinction: Biotic and Environmental Events*. (Norton, New  
801 York), 139-171.
- 802 Robertson, D., Pokorný, P., Granvik, M., Wheeler, L., & Rumpf, C. (2021). Latitude variation of flux and  
803 impact angle of asteroid collisions with earth and the moon. *Planetary Science Journal*, 2, 88.  
804 <https://doi.org/10.3847/PSJ/abefda>
- 805 Rudnick, D. L., et al. (2003), From tides to mixing along the Hawaiian Ridge, *Science*, 301(5631), 355–  
806 357. <https://doi.org/10.1126/science.1085837>
- 807 Sanford, J. C., Snedden, J.W., & Gulick, S.P.S. (2016). The Cretaceous-Paleogene boundary deposit in  
808 the Gulf of Mexico: Large-scale oceanic basin response to the Chicxulub impact. *Journal of*  
809 *Geophysical Research, Solid Earth*, v. 121 (3), 1240-1261. <https://doi.org/10.1002/2015JB012615>
- 810 Schroeder, W. (1984). The empirical age-depth relation and depth anomalies in the Pacific Ocean  
811 Basin. *Journal of Geophysical Research* 89, 9873-9883, <https://doi.org/10.1029/JB089iB12p09873>.
- 812 Schulte, P., Alegret, L., Arenillas, I., Arz, J. A., Barton, P. J., Bown, P. R., et al. (2010). The Chicxulub  
813 asteroid impact and mass extinction at the Cretaceous-Paleogene boundary. *Science (New York, N.Y.)*,  
814 327(5970), 1214–1218, <https://doi.org/10.1126/science.1177265>
- 815 Schulte, P., Speijer, R., Mai, H., & Kontny, A. (2006). The Cretaceous–Paleogene (K–P) boundary at  
816 Brazos, Texas: Sequence stratigraphy, depositional events and the Chicxulub 903 impact. *Sedimentary*  
817 *Geology*, 184, 77-109.
- 818 Schulte, P., Speijer, P., Brinkhuis, H., Kontny, A., Claeys, P., Galeotti, S., & Smit, J. (2008). Comment  
819 on the paper “Chicxulub impact predates K–T boundary: New evidence from Brazos, Texas” by Keller  
820 et al., 2008: *Earth and Planetary Science Letters*, 269, 614-620.
- 821 Scotese, C. R. (1997). *The PALEOMAP Project: paleogeographic atlas and plate tectonic*  
822 *software*. <https://cmr.earthdata.nasa.gov/search/concepts/C1214607516-SCIOPS>
- 823 Sissingh, W. (1977). Biostratigraphy of Cretaceous calcareous nannoplankton. *Geologie en Mijnbouw*, v.  
824 56(1), 37-65.
- 825 Smit, J., Roep, T.B., Alvarez, W., Montanari, A., Claeys, P., Grajales-Nishimura, J.M., & Bermudez, J.  
826 (1996). Coarse-grained, clastic sandstone complex at the K/T boundary around the Gulf of Mexico:  
827 Deposition by tsunami waves induced by the Chicxulub impact. *Geological Society of America Special*  
828 *Paper 307*, 151–182.
- 829 Smith, W.H.F., Scharroo, R., Titov, V.V., Arcas, D., & Arbic, B.K. (2005). Satellite Altimeters Measure  
830 Tsunami—Early Model Estimates Confirmed. *Oceanography*, 18(2), 11–13.  
831 <https://doi.org/10.5670/oceanog.2005.62>.

- 832 Smith, W.H.F., & Sandwell, D.T. (1997). Global seafloor topography from satellite altimetry and ship  
833 depth soundings. *Science*, 277, 1956-1962. <https://doi.org/10.1126/science.277.5334.1956>.
- 834 Stinnesbeck, W., Keller, G., de la Cruz, J., de León, C., MacLeod, N., & Whittaker, J.E. (1997). The  
835 Cretaceous–Tertiary transition in Guatemala: limestone breccia deposits from the South Peten basin.  
836 *Geologische Rundschau*, 86, 686-709.
- 837 Synolakis, C.E., Bernard, E.N., Titov, V.V., Kânoğlu, U., & González, F.I. (2008). Validation and  
838 verification of tsunami numerical models. *Pure and Applied Geophysics*, 165, 2197–2228.  
839 <https://doi.org/10.1007/s00024-004-0427-y>.
- 840 Tang, L., et al. (2012), Direct energy estimation of the 2011 Japan tsunami using deep-ocean pressure  
841 measurements, *Journal of Geophysical Research*, 117, C08008,  
842 <https://doi.org/10.1029/2011JC007635>
- 843 Titov, V.V., & Synolakis, C.E. (1995) Modeling of breaking and nonbreaking long-wave evolution and  
844 runup using VTCS–2. *Journal of Waterway, Port, Coastal and Ocean Engineering*, 121, 308-316,  
845 [https://doi.org/10.1061/\(ASCE\)0733-950X\(1995\)121:6\(308\)](https://doi.org/10.1061/(ASCE)0733-950X(1995)121:6(308))
- 846 Titov, V.V., Kânoğlu, U., & Synolakis, C. (2016): Development of MOST for real-time tsunami  
847 forecasting. *Journal of Waterway, Port, Coastal and Ocean Engineering*, 142(6), 03116004,  
848 [https://doi.org/10.1061/\(ASCE\)WW.1943-5460.0000357](https://doi.org/10.1061/(ASCE)WW.1943-5460.0000357)
- 849 Titov, V.V., Rabinovich, A.B., Mofjeld, H.O., Thomson, R.E., & González, F.I. (2005): The global reach  
850 of the 26 December 2004 Sumatra Tsunami. *Science*, 309(5743), 2045–2048,  
851 <https://doi.org/10.1126/science.1114576>
- 852 Toon, O.B., Pollack, J.B., Ackerman, T.P., Turco, R.P., McKay, C.P., and Liu, M.S. (1982). Evolution of  
853 an impact-generated dust cloud and its effects on the atmosphere. In L. T. Silver, and P. H. Schultz,  
854 (Eds.), Geological implications of impacts of large asteroids and comets on Earth. *Geological Society  
855 of America Special Paper 190*, 187–200.
- 856 Van Dorn, W.G., Le Méhauté, B., Hwang. L.-S. (1968). Handbook of explosion-generated water  
857 waves. Report TC-130. Tetra Tech Inc., Pasadena, CA.
- 858 Ward, S. (2012), Chicxulub Tsunami.mov, *YouTube*. Available from:  
859 <https://www.youtube.com/watch?v=Dcp0JhwNgmE>  
860
- 861 Ward, S. (2021), Chicxulub Tsunami-2.mov, *YouTube*. Available from:  
862 <https://www.youtube.com/watch?v=5qhqmXMUu6U&t=31s>  
863
- 864 Weiss, R., Wünnemann, K., & Bahlburg, H. (2006). Numerical modelling of generation, propagation and  
865 run-up of tsunamis caused by oceanic impacts: model strategy and technical solutions. *Geophysical  
866 Journal International*, 167, 77-88. <https://doi.org/10.1111/j.1365-246X.2006.02889.x>  
867
- 868 Weiss, R., and Wünnemann, K. (2007). Large waves caused by oceanic impacts of meteorites. In *Tsunami  
869 and Nonlinear Waves* (pp. 237-261). Springer, Berlin, Heidelberg.  
870

- 871 Wünnemann, K., Collins, G. S., and Weiss, R. (2010). Impact of a cosmic body into Earth's ocean and the  
872 generation of large tsunami waves: insight from numerical modeling. *Reviews of Geophysics*, 48,  
873 RG4006, <https://doi.org/10.1029/2009RG000308>  
874
- 875 Westerhold, T., Röhl, U., and Laskar, J. (2012). Time scale controversy: accurate orbital calibration of the  
876 Early Paleogene. *Geochemistry, Geophysics, Geosystems*, 13, 73-82.  
877 <http://dx.doi.org/10.1029/2012gc004096>.  
878
- 879 Wünnemann, K., & Weiss, R. (2015). The meteorite impact-induced tsunami hazard. *Philosophical*  
880 *Transactions of the Royal Society A: Mathematical, Physical and Engineering Sciences*, 373(2053).  
881 <https://doi.org/10.1098/rsta.2014.0381>
- 882 Wünnemann, K., Collins, G.S., & Melosh, H.J. (2006). A strain-based porosity model for use in hydrocode  
883 simulations of impacts and implications for transient crater growth in porous targets. *Icarus*, 180(2),  
884 514–527. <https://doi.org/10.1016/j.icarus.2005.10.013>
- 885 Wunsch, C., & R. Ferrari (2004), Vertical mixing, energy, and the general circulation of the oceans,  
886 *Annual Reviews of Fluid Mechanics*, 36, 281–314.
- 887 Zhou, H., Wei, Y., & Titov, V.V. (2012): Dispersive modeling of the 2009 Samoa tsunami. *Geophysical*  
888 *Research Letters*, 39, L16603, <https://doi.org/10.1029/2012GL053068>

889 **References in Supplementary Tables ST-1 and ST-2**

- 890
- 891 Abramovich, S., Keller, G., Adatte, T., Stinnesbeck, W., Hottinger, L., Stüben, D., Berner, Z.,  
892 Ramanivosoa, B. & Randriamanantenaso, A. (2002). Age and paleoenvironment of the Maastrichtian-  
893 Paleocene of the Mahajanga Basin, Madagascar: a multidisciplinary approach. *Marine*  
894 *Micropaleontology* 47, 17–70. [http://dx.doi.org/10.1016/S0377-](http://dx.doi.org/10.1016/S0377-8398(02)00094-4) 8398(02)00094-4. FIX DOI; should be  
895 clickable  
896
- 897 Açıklın, S, Vellekoop, J., Ocakoglu, F., Yılmaz, I.Ö., Smit, J., Altner, S. Ö., Goderis, S, Vonhof, H.,  
898 Speijer, R.P., Woelders, L., Fornaciari, E., & Brinkhuis, H. (2015). Geochemical and palaeontological  
899 characterization of a new K-Pg Boundary locality from the Northern branch of the Neo-Tethys:  
900 Mudurnu e Göynük Basin, NW Turkey: *Cretaceous Research*, 52, 251-267.  
901
- 902 Adatte, T., Keller, G., Burns, S., Stoykova, K.H., Ivanov, M.I., Vangelov, D., Kramar, U., & Stüben, D.  
903 (2016). Paleoenvironment across the Cretaceous-Tertiary transition in eastern Bulgaria: *Geological*  
904 *Society of America Special Paper* 356, 231-251.  
905
- 906 Alegret, L., Arenillas, I., Diaz, C., Grajales-Nishimura, J., Meléndez, A., Molina, E., Rojas Museo, R., &  
907 Soria, A.R. (2005). Cretaceous-Paleogene boundary deposits at Loma Capiro, central Cuba: Evidence  
908 for the Chicxulub impact. *Geology*, 33 (9), 721-724.  
909
- 910 Alegret, L., Thomas, E, & Lohmann, K.C. (2012). End-Cretaceous marine mass extinction not caused by  
911 productivity collapse. *Proceedings of the National Academy of Sciences of the United States of America*  
912 109(3), 728-732.  
913
- 914 Alegret, L., Kaminski, M.A., & Molina, E. (2004). Paleoenvironmental recovery after the  
915 Cretaceous/Paleogene boundary crisis: evidence From the marine Bidart section (SW France). *Palaios*,

916 19, 574-586.  
917  
918 Alvarez, W., Asaro, F. & Montanari, A. (1990). Iridium profile for 10 million years across the Cretaceous-  
919 Tertiary Boundary at Gubbio (Italy). *Science*, 250, 1700-1702.  
920  
921 Alvarez, W. & Lowrie, W. (1979). Upper Cretaceous palaeomagnetic stratigraphy at Moria, Umbrian  
922 Apennines, Italy: verification of the Gubbio section: *Geophysical Journal of the Royal Astronomical*  
923 *Society*, 57, 1-17.  
924  
925 Andrews, J.E., Packham, G., et al. (1975). *Initial Reports of the Deep Sea Drilling Project, Volume 30*.  
926 Washington DC: U.S. Govt. Printing Office.  
927  
928 Arnth, J.-D, Matzigkeit, U., & Boos, A. (1985). Carbon isotope geochemistry of the Cretaceous-Tertiary  
929 section of the Wasserfallgraben, Lattengebirge, southeast Germany. *Earth and Planetary Science*  
930 *Letters*, 75, 50-58.  
931  
932 Askin, R. A. (1985). The palynological record across the Cretaceous/Tertiary transition on Seymour  
933 Island, Antarctica. In R.M. Feldmann, M.O. Woodburne, (Eds.), *Geology and paleontology of Seymour*  
934 *Island: Geological Society of America Memoir 169*, (pp. 155-162).  
935  
936 Austin, J. A., Jr., Schlager, W., Palmer, A.A. et al. (1986). *Proceedings of the Ocean Drilling Program,*  
937 *Initial Reports. (Pt. A), 101*. College Station, TX: Ocean Drilling Program.  
938  
939 Barker, P. F., Dalziel, I.W.D., et al. (1976). *Initial Reports of the Deep Sea Drilling Project 36*.  
940 Washington DC: U.S. Govt. Printing Office.  
941  
942 Barker, P. F., Carlson, R.L., & Johnson, D.A. (1983). *Initial Reports Deep Sea Drilling Program, 72*.  
943 Washington DC: U.S. Govt. Printing Office.  
944  
945 Barker, P. F., Kennett, J.P., et al. (1988). *Proceedings of the Ocean Drilling Program, Initial Reports, 113*.  
946 College Station, TX: Ocean Drilling Program.  
947  
948 Barker, P. F., Kennett, J.P., et al. (1990), *Proceedings of the Ocean Drilling Program, Scientific Results,*  
949 *113*. College Station, TX: Ocean Drilling Program.  
950  
951 Barrera, E. (1994). Global environmental changes preceding the Cretaceous-Tertiary boundary: Early-late  
952 Maastrichtian transition: *Geology*, 22, 877-880,  
953  
954 Barron, J., Larsen, B., et al.. 1989, *Proceedings of the Ocean Drilling Program, Initial Reports, 119*.  
955 College Station, TX: Ocean Drilling Program.  
956  
957 Benson, W. E., Sheridan, R. E., et al. (1978). *Initial Reports of the Deep Sea Drilling Project,*  
958 *44*. Washington DC: U.S. Govt. Printing Office), 1005 pp.  
959  
960 Bleil, U., (2007). The magnetostratigraphy of northwest Pacific sediments, Deep Sea Drilling Project Leg  
961 86. In G. R. Heath, L. H. Burckle et al., *Initial Reports of the Deep Sea Drilling Project, 86*.  
962 Washington DC: U.S. Govt. Printing Office.  
963  
964 Boillot, G., Winterer, E.L., Meyer, A.W., et al. (1987). *Proceedings of the Ocean Drilling Program, Initial*

- 965        *Reports, (Pt. A) 103*. College Station, TX: Ocean Drilling Program.  
966
- 967 Bolli, H. M., Ryan, W.B.F. et al. (1978 *Initial Reports of the Deep Sea Drilling Project, Volume 40*.  
968        Washington DC: U.S. Govt. Printing Office.  
969
- 970 Bowles, J. (2007). Data report: revised magnetostratigraphy and magnetic mineralogy of sediments from  
971        Walvis Ridge, Leg 208 In D. Kroon, D., J.C. Zachos, C. Richter. (Eds.): *Proceedings of the Ocean*  
972        *Drilling Program, Scientific Results, 208*. (College Station, TX: Ocean Drilling Program), 24 pp.  
973        doi:10.2973/odp.proc.sr.208.2007 .  
974
- 975 Bowman, V.C., Francis, J.E., Askinb, R.A., Riding, J.B., & Swindles, G.T. (2014, Latest Cretaceous–  
976        earliest Paleogene vegetation and climate change at the high southern latitudes: palynological evidence  
977        from Seymour Island, Antarctic Peninsula.  
978
- 979 Bralower, T.J., & Siesser, W.G. (1992). Cretaceous calcareous nannofossil biostratigraphy of Sites  
980        761, 762, and 763, Exmouth and Wombat Plateaus, Northwest Australia. In U. von Rad, B.U.  
981        Haq, et al.: *Proceedings of the Ocean Drilling Program, Initial Reports, 122*. College Station, TX,  
982        Ocean Drilling Program.  
983
- 984 Bralower, T.J., Premoli Silva, I., Malone, M.J. et al. (2002a). *Proceedings of the Ocean Drilling*  
985        *Program, Initial Reports, (Pt. A), 198*. College Station, TX: Ocean Drilling Program.  
986        doi:10.2973/odp.proc.ir.198.2002,  
987
- 988 Bralower, T.J., Premoli Silva, I., & Malone, M.J. (2002b). Leg 198 synthesis: a remarkable 120 M.Y.  
989        record of climate and ceanography from Shatsky Rise, Northwest Pacific Ocean, In T.J. Bralower, I.  
990        Premoli Silva, M.J. Malone, et al. *Proceedings of the Ocean Drilling Program, Initial Reports, 198*.  
991        College Station, TX: Ocean Drilling Program. doi:10.2973/odp.proc.ir.198.2002, p. 1-47.  
992
- 993 Brinkhuis, H. & Zachariasse, W.J. (1988). Dinoflagellate cysts, sea level changes and planktonic  
994        foraminifers across the Cretaceous-Tertiary boundary at El Haria, Northwest Tunisia. *Marine*  
995        *Micropaleontology, 13*, 153-191.  
996
- 997 Buffler, R. T., Schlager, W. et al. (1984). *Initial Reports of the Deep Sea Drilling Project, 11*.  
998        Washington DC: U.S. Govt. Printing Office.  
999
- 1000 Burns, R. E., Andrews, J.E. et al. (1973). *Initial Reports of the Deep Sea Drilling Project, 21*.  
1001        Washington DC: U.S. Govt. Printing Office.  
1002
- 1003 Carter, R.M., McCave, I.N., Richter, C., Carter, L., et al. (1999). *Proceedings of the Ocean Drilling*  
1004        *Program, Initial Reports, 181* [Online]. doi:10.2973/odp.proc.ir.181.2000, Available from World Wide  
1005        Web: <[http://www-odp.tamu.edu/publications/181\\_IR/181ir.htm](http://www-odp.tamu.edu/publications/181_IR/181ir.htm)>.  
1006
- 1007 Clemens, S.C., Kuhnt, W., LeVay, L.J., & the Expedition 353 Scientists. (2015). *Expedition 353*  
1008        *Preliminary Report: Indian Monsoon Rainfall*. International Ocean Discovery  
1009        Program. <http://dx.doi.org/10.14379/iodp.pr.353.2015>.  
1010
- 1011 Ciesielski, P. F., Kristoffersen, Y. et al. (1988). *Proceedings of the Ocean Drilling Program, Initial*  
1012        *Reports, 114*. College Station, TX: Ocean Drilling Program.  
1013



- 1014 Coffin, M.F., Frey, F.A., Wallace, P.J. et al. (2000). *Proceedings of the Ocean Drilling Program, Initial*  
1015 *Reports, 183* [Online]. doi:10.2973/odp.proc.ir.183.2000, Available from World Wide Web:  
1016 <[http://www-odp.tamu.edu/publications/183\\_IR/183ir.htm](http://www-odp.tamu.edu/publications/183_IR/183ir.htm)>.  
1017
- 1018 Creager, J. S., Scholl, D.W. et al. (197). *Initial Reports of the Deep Sea Drilling Project*. Washington DC:  
1019 U.S. Govt. Printing Office), 930 pp.  
1020
- 1021 Davies, T. A., Luyendyk, B.P. et al. (1974). *Initial Reports of the Deep Sea Drilling Project, 26*.  
1022 Washington DC: U.S. Govt. Printing Office.  
1023
- 1024 Dinarès-Turell, J., Westerhold, T., Victoriano Pujalte, V., Röhl, U. & Kroon, D. (2013). Settling the  
1025 Danian astronomical time scale: a prospective global unit stratotype at Zumaia, Basque Basin. In R.  
1026 Rocha et al., (Eds), *STRATI 2013*. Springer International Publishing Switzerland. doi: 10.1007/978-3-  
1027 319-04364-7\_38  
1028
- 1029 Donovan, A.D., Baum, G.R., Blechschmidt, G.L., Loutit, T.S., Pflum, C.E. & Vail, P.R. (2012). Sequence  
1030 Stratigraphic Setting of the Cretaceous-Tertiary boundary in central Alabama. In Sea-Level Changes-  
1031 An Integrated Approach, *SEPM Society for Sedimentary Geology Special Publication No. 42*, 299-307.  
1032
- 1033 Edgar, N. T., Saunders, J.B. et al. (1973). *Initial Reports of the Deep Sea Drilling Project,*  
1034 *15*. Washington DC: U.S. Govt. Printing Office.  
1035
- 1036 Elliot . D.H., Askin, R.A., Kyte, F.T, & Zinsmeister, W. J. (1994). Iridium and dinocysts at the  
1037 Cretaceous-Tertiary boundary on Seymour Island, Antarctica: Implications for the K-T event: *Geology*,  
1038 *22*, 675-678.  
1039
- 1040 Erbacher, J., Mosher, D.C., Malone, M.J. et al. (2004). *Proceedings of the Ocean Drilling Program,*  
1041 *Initial Reports, 207*. College Station, TX: Ocean Drilling Program. doi:10.2973/odp.proc.ir.207.2004.  
1042
- 1043 Esmeray-Senlet, S., Wright, J.D., Olsson, R.K., Miller, K.G., Browning, J.V. & Quan, T.M. (2015).  
1044 Evidence for reduced export productivity following the Cretaceous/Paleogene mass extinction:  
1045 *Paleoceanography, 30*, 718–738. doi:10.1002/2014PA002724.  
1046
- 1047 Exon, N.F., Kennett, J.P., & Malone, M.J. (2004). Leg 189 synthesis: Cretaceous–Holocene history of the  
1048 Tasmanian Gateway. In N.F. Exon, J.P. Kennett, and M.J. Malone, (Eds.). *Proceedings of the Ocean*  
1049 *Drilling Program, Scientific Results, 189*, 1-37. College Station, TX: Ocean Drilling Program.  
1050 doi:10.2973/odp.proc.sr.189.101.2004  
1051
- 1052 Galburn, B. (1992). Magnetostratigraphy of Upper Cretaceous and Lower Tertiary sediments, Sites 761  
1053 and 762, Exmouth Plateau, Northwest Australia. In U. von Rad, B.U. Haq, et al. *Proceedings of the*  
1054 *Ocean Drilling Program, Scientific Results, 122*: College Station, TX: Ocean Drilling Program.  
1055
- 1056 Galbrun, B., and Gardin, S. (2004). New chronostratigraphy of the Cretaceous–Paleogene boundary  
1057 interval at Bidart, France: *Earth and Planetary Science Letters, 224*, 19-32.  
1058
- 1059 Graciansky, P. C. de, Poag, C.W. et al. (1985). *Initial Reports of the Deep Sea Drilling Project, 80*.  
1060 Washington DC: U.S. Govt. Printing Office.  
1061
- 1062 Hailwood, E.A. & Clement, B.M. (1991). Magnetostratigraphy of Sites 699 and 700, East Georgia Basin.

1063 In P. F. Ciesielski, Y. Kristoffersen, et al. *Proceedings of the Ocean Drilling Program, Scientific*  
1064 *Results, 114*. College Station, TX: Ocean Drilling Program. 337-357.  
1065  
1066 Hamilton, N. (1990). Mesozoic magnetostratigraphy of Maud Rise, Antarctica, In P.F. Barker, J.P.  
1067 Kennett, et al. *Proceedings of the Ocean Drilling Program, Scientific Results, 113*. College Station, TX:  
1068 Ocean Drilling Program.  
1069  
1070 Hamilton, N. & Suzyumov, A. E. (1983). Late Cretaceous magnetostratigraphy of Site 516, Rio Grande  
1071 Rise, southwestern Atlantic Ocean, Deep Sea Drilling Project, Leg 72. In P.F. Barker, R.L. Carlson, and  
1072 D.A. Johnson: *Initial Reports of the Deep Sea Drilling Project, 72*. Washington DC: U.S. Govt.  
1073 Printing Office, 723-730.  
1074  
1075 Hansen. J. M. (1979). Dinoflagellate zonation around the boundary. In T. Birkelund, & R. G. Bromley,  
1076 (Eds.). *Cretaceous-Tertiary boundary events. Volume I*. (University of Copenhagen, Denmark), 136-  
1077 141.  
1078  
1079 Hansen, H.J., Drobne, K., & Gwozdz, R. (1995). The K/T boundary in Slovenia: Dating by magnetic  
1080 susceptibility and an iridium anomaly in a debris flow: 4th Int. workshop European Science Network  
1081 "Impact Cratering and Evolution of Planet Earth", Ancona, May 1995, Abstracts and Field Trips.  
1082 (Università degli Studi Urbino, Ancona) 84–85.  
1083  
1084 Haq, B.U., von Rad, U., O'Connell, S. et al., (1990). *Proceedings of the Ocean Drilling Program, Initial*  
1085 *Reports, 122*. College Station, T X: Ocean Drilling Program).  
1086  
1087 Hart, M.B., Feist, S.E., Håkanssonc, E., Heinbergd, C., Price, G.D., Lenge, M.J., & Watkinson, M. P.  
1088 (2005). The Cretaceous–Palaeogene boundary succession at Stevns Klint, Denmark: Foraminifers and  
1089 stable isotope stratigraphy: *Palaeogeography, Palaeoclimatology, Palaeoecology, 224*), 6 – 26.  
1090  
1091 Hay, W. W., Sibuet, J.-C. et al. (1984). *Initial Reports of the Deep Sea Drilling Project, 75*.  
1092 Washington DC: U.S. Govt. Printing Office.  
1093  
1094 Hayes, D. E., Pimm, A.C. et al. (1972). *Initial Reports of the Deep Sea Drilling Project, 14*. Washington  
1095 DC: U.S. Government Printing Office.  
1096  
1097 Hayes, D. E., Frakes, L.A. et al. (1975). *Initial Reports of the Deep Sea Drilling Project, 28*.  
1098 Washington DC: U.S. Govt. Printing Office.  
1099  
1100 Heath, G. R., Burckle, L.H. et al. (1985). *Initial Reports of the Deep Sea Drilling Project, 86*.  
1101 Washington DC: U.S. Govt. Printing Office.  
1102  
1103 Herbert, T.D. & D'Hondt, S.L. (1990). Precessional climate cyclicity in Late Cretaceous-Early Tertiary  
1104 marine sediments: a high resolution chronometer of Cretaceous-Tertiary boundary events. *Earth and*  
1105 *Planetary Science Letters, 99*, 263-275.  
1106  
1107 Hinz, K., Winterer, E.L. et al. (1984). *Initial Reports of the Deep Sea Drilling Project, 79*.  
1108 Washington DC: U.S. Govt. Printing Office.  
1109  
1110 Hollis, C.J. (2002). Biostratigraphy and paleoceanographic significance of Paleocene radiolarians from  
1111 offshore eastern New Zealand. *Marine Micropaleontology, 46*, 265-316.

1112  
1113 Hollis, C. J. , Strong , C. P., Rodgers, K. A., & Rogers, K. M. (2003). Paleoenvironmental changes across  
1114 the Cretaceous/Tertiary boundary at Flaxbourne River and Woodside Creek, eastern Marlborough: New  
1115 Zealand. *New Zealand Journal of Geology and Geophysics*, 46, 177-197.  
1116  
1117 Hollister, C. D., Craddock, C. et al. (1976). *Initial Reports of the Deep Sea Drilling Project*, 35.  
1118 Washington DC: U.S. Government Printing Office.  
1119  
1120 Hsü, K. J., and LaBrecque, J.L. et al. (1984). *Initial Reports of the Deep Sea Drilling Project*, 73.  
1121 Washington (U.S. Govt. Printing Office).  
1122  
1123 Huber, B.T., Liu, C., Olsson, R.K. & Berggren, W.A. (1994). Comment on "The Cretaceous-Tertiary  
1124 boundary transition in the Antarctic Ocean and its global implications", by G. Keller: *Marine*  
1125 *Micropaleontology*, 24, 91-99.  
1126  
1127 Keller, G., Adatte, T. , Stinnesbeck, W., Stüben, D., Kramar, U., Berner, Z., Li, L., & Perch-Nielsen, K. v.  
1128 S. (1998). The Cretaceous-Tertiary transition on the shallow Saharan Platform of Southern Tunisia.  
1129 *Geobios*, 30, 951-975.  
1130  
1131 Keller, G., Adatte, T., Tantawy, A.A., Berner, Z., Stüben, D. (2007). High stress late Cretaceous to early  
1132 Danian paleoenvironment in the Neuquen Basin, Argentina. *Cretaceous Research*, 28, 939–960.  
1133 <http://dx.doi.org/10.1016/j.cretres.2007.01.006>.  
1134  
1135 Keller, G., Khozyem, H.M., Adatte, T., Malarkodi, N., Spangenberg, J.E., Stinnesbeck, W. (2013,).  
1136 Chicxulub impact spherules in the North Atlantic and Caribbean: age constraints and Cretaceous-  
1137 Tertiary boundary hiatus. *Geological Magazine* 150, 885–907.  
1138 <http://dx.doi.org/10.1017/S0016756812001069>.  
1139  
1140 Kroenke, L. W., Berger, W.H., Janecek, T.R. et al. (1991). *Proceedings of the Ocean Drilling Program*,  
1141 *Initial Report*, 130. College Station, TX: Ocean Drilling Program.  
1142  
1143 Kyte, F.T., Smit, J. & Wasson, J.T. (1985). Siderophile interelement variations in the Cretaceous-Tertiary  
1144 boundary sediments from Caravaca, Spain. *Earth and Planetary Science Letters*, 73, 183-195.  
1145  
1146 Lancelot, Y., Winterer, E.L. (1980). *Initial Reports of the Deep Sea Drilling Project*, 50. Washington DC:  
1147 U.S. Government Printing Office.  
1148  
1149 Lancelot, Y., Seibold, E. et al. (1977). *Initial Reports of the Deep Sea Drilling Project*, 41. Washington  
1150 DC: U.S. Government Printing Office.  
1151  
1152 Landman, N.H., Johnson, R.O., Garb, M.P., Edwards, L.E., & Kyte, F.T. (2007). Tertiary boundary  
1153 interval on the Atlantic coastal plain, with a description of the highest ammonite zones in North  
1154 America. Part III. Manasquan River Basin, Monmouth County, New Jersey. *Bulletin of the American*  
1155 *Museum Natural History*, 30, 122 pp.  
1156  
1157 Larson, R. L., Moberly, R. et al. (1975). *Initial Reports of the Deep Sea Drilling Project*, 32. Washington  
1158 DC: U.S. Government Printing Office.  
1159  
1160 Latal, C. (2004). The Cretaceous-Paleogene boundary section of Gorgo a Cerbara: an integrated

1161 stratigraphical study. *Annals Naturhistorisches Museum Wien*, 160A, 259-279.  
1162  
1163 Ludwig, W. J., Krasheninikov, V.A. et al. (1983). *Initial Reports of the Deep Sea Drilling Project*, 71.  
1164 Washington DC: U.S. Government Printing Office.  
1165  
1166 MacLeod, K.G.& Keller, G. (1991a). How complete are Cretaceous/Tertiary boundary sections? A  
1167 chronostratigraphic estimate based on graphic correlation. *Geological Society of America Bulletin*, 103,  
1168 1439-1457.  
1169  
1170 MacLeod, K.G.& Keller, G. (1991b). Hiatus distributions and mass extinctions at the Cretaceous/Tertiary  
1171 boundary. *Geology*, 19, 497-501.  
1172  
1173 Mahoney, J.J., Fitton, J.G., Wallace, P.J. et al. (2001). *Proceedings of the Ocean Drilling Program, Initial*  
1174 *Reports 19*. College Station, TX, Ocean Drilling Program. doi.10.2973/odp.proc.ir.192.2001.  
1175  
1176 Mateo, P., Keller, G., Adatte. T. & Spangenberg., J.E. (2016). Mass wasting and hiatuses during the  
1177 Cretaceous-Tertiary transition in the North Atlantic: Relationship to the Chicxulub impact.  
1178 *Palaeogeography, Palaeoclimatology, Palaeoecology*. 441, 96–115.  
1179 <http://dx.doi.org/10.1016/j.palaeo.2015.01.019>  
1180  
1181 Mascle, J., Lohmann, G.P., Clift, P.D. et al. (1996). *Proceedings of the Ocean Drilling Program, Initial*  
1182 *Reports*, 159. College Station, TX, Ocean Drilling Program.  
1183  
1184 Maxwell, A. E. et al. (1970). *Initial Reports of the Deep Sea Drilling Project*, 3. Washington DC: U.S.  
1185 Government Printing Office.  
1186  
1187 Miller, K.G., Sugarman, P.J., Browning, J.V. et al. (1998). Bass River Site report. *Scientific results, Ocean Drilling*  
1188 *Program, Leg 174AX Supplement*, 5-43. College Station, TX: Ocean Drilling Program.  
1189 10.2973/odp.proc.ir.174AX.1998  
1190  
1191 Miller, K.G., Sugarman, P.J., Browning, J.V. et al. (1999). *Proceedings of the Ocean Drilling Program,*  
1192 *Initial Reports , 174AX (Suppl.)*. College Station, TX: Ocean Drilling Program.  
1193 doi:10.2973/Odp.Proc.Ir.174axs.104.1999.  
1194  
1195 Moberly, R., Schlanger, S.O. et al. (1986). *Initial Reports of the Deep Sea Drilling Project*, 89. Washington DC:  
1196 U.S. Government Printing Office.  
1197  
1198 Molina, E., Alegret<sup>1</sup>, L., Arenillas<sup>1</sup>, I., Arz<sup>1</sup>, J.A., Gallala, N., Hardenbol, J., von Salis, K., Steurbaut<sup>5</sup>, E.,  
1199 Vandenberghe, N. & Zaghbib-Turki, D. (2006). The Global Boundary Stratotype Section and Point for the base  
1200 of the Danian Stage (Paleocene, Paleogene, "Tertiary", Cenozoic) at El Kef, Tunisia Original definition and  
1201 revision. *Episodes*, 29(4), 263-273.  
1202  
1203 Molina, E., Alegret, L., Arenillas, I., and Arz, J. A. (2005). The Cretaceous/Paleogene boundary at the Agost section  
1204 revisited: paleoenvironmental reconstruction and mass extinction pattern: *Journal Iberian Geology*, 31 (I), 135-  
1205 150.  
1206  
1207 Montadert, L., Z, & Roberts, D.G. (1979). *Initial Reports of the Deep Sea Drilling Project*, 48.  
1208 Washington DC: U.S. Government Printing Office.  
1209

- 1210 Montanari, A., Hay, R.L., Alvarez, W., Asaro, F., Michel, H.V., Alvarez, L.W. & Smit, J. (1983). Spheroids at the  
1211 Cretaceous-Tertiary boundary are altered impact droplets of basaltic composition: *Geology*, *11*, 668-671.  
1212
- 1213 Moore, T. C, Jr., Rabinowitz, P.D. et al. (1984). *Initial Reports of the Deep Sea Drilling Project*, 7.  
1214 Washington DC: U.S. Government Printing Office.  
1215
- 1216 Michel, H.V., Asaro, F., Alvarez, W. Z & Alvarez L.W. (1990). Geochemical studies of the Cretaceous-  
1217 Tertiary boundary in ODP holes 689b and 690c. In P.F. Barker, J.P. Kennett, et al: *Proceedings of the*  
1218 *Ocean Drilling Program, Scientific Results, 113*. College Station, TX: Ocean Drilling Program, 159-  
1219 168.  
1220
- 1221 Norris, R.D., Kroon, D., Klaus, A., et al. (1998). *Proceedings of the Ocean Drilling Program, Initial*  
1222 *Reports, 171B*. College Station, TX: Ocean Drilling Program.  
1223
- 1224 Ogorelec, B, Dolenc, T., & Drobne, K. (2007). Cretaceous–Tertiary boundary problem on shallow  
1225 carbonate platform: Carbon and oxygen excursions, biota and microfacies at the K/T boundary sections  
1226 Dolenja Vas and Sopada in SW Slovenia, Adria CP. *Palaeogeography, Palaeoclimatology,*  
1227 *Palaeoecology*, *255*, 64–76.  
1228
- 1229 Olsson, R.K., Miller, K.G., Browning, J.V., Wright, J.D., & Cramer, B.S. (2002). Sequence stratigraphy  
1230 and sea level change across the Cretaceous/Tertiary boundary on the New Jersey passive margin. In C.  
1231 Koeberl and K.G. MacLeod, K.G., (Eds.) *Catastrophic Events and Mass Extinctions: Impacts and*  
1232 *Beyond, Geological Society of America Special Paper 356*, 97–108.  
1233
- 1234 Olsson, R.K., Miller, K.G., Browning, J.V., Habib, D., & Sugarman, P.J. (1997). Ejecta layer at the  
1235 Cretaceous-Tertiary boundary, Bass River, New Jersey (Ocean Drilling Program Leg 174AX). *Geology*,  
1236 *25*(8),759–762.  
1237
- 1238 Peirce, J., Weissel, J. et al. (1989). *Proceedings of the Ocean Drilling Program, Initial Reports, 121*.  
1239 College Station, TX: Ocean Drilling Program.  
1240
- 1241 Perch Nielsen, K., McKenzie, J., Quziang, H.E., Silver, L.T., & Schultz, P.H. (1982). Biostratigraphy and  
1242 isotope stratigraphy and the "catastrophic" extinction of calcareous nannoplankton at the  
1243 Cretaceous/Tertiary boundary: *Geological Society of America Special Paper, 190*, 353-371.  
1244
- 1245 Poore, R., Tauxe, L., Percival Jr., S.F., Labrecque, J.L., Wright, R., Petersen, N.Y.P., Smith, C.C., Tucker,  
1246 P. & Hsu, K.J. (1983). Late Cretaceous-Cenozoic Magnetostratigraphic and biostratigraphic  
1247 correlations of The South Atlantic Ocean: DSDP Leg 73: *Palaeogeography, Palaeoclimatology,*  
1248 *Palaeoecology*, *42*, 127-149.  
1249
- 1250 Premoli Silva, I., Haggerty, J., Rack, F. et al. 1993). *Proceedings of the Ocean Drilling Program, Initial*  
1251 *Reports, 144*. College Station, TX: Ocean Drilling Program.  
1252
- 1253 Punekar, J., Keller, G., Khozyem, H.M., Adatte, T., Font, E., & Spangenberg, J. (2016). A multi-proxy  
1254 approach to decode the end-Cretaceous mass extinction: *Palaeogeography, Palaeoclimatology,*  
1255 *Palaeoecology*, *441*, 116-136.  
1256
- 1257 Rea, D.K., Basov, L.A., Janecek, T.R., Palmer-Julson, A. et al. (1993). *Proceedings of the Ocean Drilling*  
1258 *Program, Initial Reports, 145*. College Station, TX: Ocean Drilling Program.

1259  
1260 Robin, E., Boclet, D., Ph. Bonte, Ph., Froget, L., C. Jehanna, C. & Rocchia. R. (1991). The stratigraphic  
1261 distribution of Ni-rich spinels in Cretaceous-Tertiary boundary rocks at El Kef (Tunisia), Caravaca  
1262 (Spain) and Hole 761C (Leg 122): *Earth and Planetary Science Letters*. V. 107 (3-4), 715-721.  
1263  
1264 Ruddiman, W., Sarnthein, M., Baldauf, J. et al. (1988). *Proceedings of the Ocean Drilling Program, Initial*  
1265 *Reports, 108 (Part A)*. College Station, TX: Ocean Drilling Program.  
1266  
1267 Sager, W.W., Winterer, E.L, Firth, J.V. et al. (1993). *Proceedings of the Ocean Drilling Program, Initial*  
1268 *Reports, 14*. College Station, TX, Ocean Drilling Program.  
1269  
1270 Saito, T., Yamanoi, T., & Kaiho, K. (1986). End-Cretaceous devastation of terrestrial flora in the boreal  
1271 Far East: *Nature*, 323, 253-255.  
1272  
1273 Schlanger, S. O., Jackson, E.D. et al., (1976). *Initial Reports of the Deep Sea Drilling Project, 33*.  
1274 Washington DC, U.S. Government Printing Office.  
1275  
1276 Schlich, R., Wise, Jr., S.W. et al. (1989). *Proceedings of the Ocean Drilling Program, Initial Reports 120*.  
1277 College Station, TX, Ocean Drilling Program.  
1278  
1279 Schmitz, B., Keller, G., & Stenvall, O., (1992). Stable isotope and foraminiferal changes across the  
1280 Cretaceous-Tertiary boundary at Stevns Klint, Denmark Arguments for long-term oceanic instability  
1281 before and after bolide-impact event: *Palaeogeography, Palaeoclimatology, Palaeoecology*, 96, 233-  
1282 260.  
1283  
1284 Sibuet, J.-C, Ryan, W.B.F., et al. (1979). *Initial Reports of the Deep Sea Drilling Project, 47 Part 2*.  
1285 Washington DC: U.S. Government Printing Office.  
1286  
1287 Sigurdsson, H., Leckie, R.M., Acton, G.D., et al. (1997) *Proceedings of the Ocean Drilling Program,*  
1288 *Initial Reports, 165*. College Sta- tion, TX: Ocean Drilling Program.  
1289  
1290 Simpson, E.S.W., Schlich, R., et al. (1974). *Initial Reports of the Deep Sea Drilling Project, 25*.  
1291 Washington DC: U.S. Government Printing Office.  
1292  
1293 Smit, J. (1999). The global stratigraphy of the Cretaceous-Tertiary boundary impact ejecta.  
1294 *Annual Review of Earth and Planetary Sciences*, 27, 75-113.  
1295  
1296 Smit, J. & Romein, A.J.T. (1985). A sequence of events across the Cretaceous-Tertiary boundary: *Earth*  
1297 *and Planetary Science Letters*, 74, 55-170.  
1298  
1299 Smit, J., Montanari, A., Swinburne, N.H.M., Alvarez, w., Hildebrand, A.R., Margolis, S.V., Claeys,  
1300 Lowrie, W., & Asaro, , F. (1992). Tektite-bearing, deep-water clastic unit at the Cretaceous-Tertiary  
1301 boundary in northeastern Mexico: *Geology*, 20, 99-103.  
1302  
1303 Storms, M.A., Natland, J.H. et al. (1991). *Proceedings of the Ocean Drilling Program, Initial Reports 132*.  
1304 CollegeStation, TX: Ocean Drilling Program.  
1305  
1306 Stott, L.D. & Kennett, J. P. (1990). the paleoceanographic and paleoclimatic signature of the

- 1307 Cretaceous/Paleogene boundary in the Antarctic: stable isotopic results from ODP leg 113. In P.F.  
1308 Barker, J.P. Kennett, et al. *Proceedings of the Ocean Drilling Program, Scientific Results, 113*. College  
1309 Station, TX: Ocean Drilling Program.  
1310
- 1311 Stüben, D., Kramar, U., Berner, Z., Stinnesbeck, W., Keller, G., & Adatte, T. (2002). Trace elements,  
1312 stable isotopes, and clay mineralogy of the Elles II K/T boundary section in Tunisia: indications for sea  
1313 level fluctuations and primary productivity. *Palaeogeography, Palaeoclimatology, Palaeoecology, 178*,  
1314 321-345.  
1315
- 1316 Saganuma, Y. & Ogg, J. G. (2006). Campanian through Eocene magnetostratigraphy of Sites 1257–1261,  
1317 OD Leg 207, Demerara Rise (western equatorial Atlantic). In D.C. Mosher, J. Erbacher, and M.J.  
1318 Malone, (Eds.), *Proceedings of the Ocean Drilling Program, Scientific Results, 207(3)*. College Station,  
1319 TX: Ocean Drilling Program. doi:10.2973/odp.proc.sr.207.102.2006  
1320
- 1321 Supko, P. R., Perch-Nielsen, K. et al. (1977). *Initial Reports of the Deep Sea Drilling Project, 39*.  
1322 Washington, DC: U.S. Government Printing Office.  
1323
- 1324 Tada, R., Iturralde-Vinent, M.A., Matsui, T., Tajika, E., Oji, T., Goto, K., Nakano, Y., Takayama, H.,  
1325 Yamamoto, S., Kiyokawa, S., Toyoda, K., Garcia-Delgado, D., Diaz-Otero, C., & Rojas-Consuegra, R.  
1326 (2003). K/T boundary deposits in the Paleo-western Caribbean basin. In C. Bartolini, R. T. Buffler, and  
1327 J. Blickwede, (Eds.), *The Circum-Gulf of Mexico and the Caribbean: Hydrocarbon habitats, basin*  
1328 *formation, and plate tectonics. American Association of Petroleum Geologists Memoir 79, 582–604*.  
1329
- 1330 Tarduno, J.A., Duncan, R.A., Scholl, D.W. et al. (2002). *Proceedings of the Ocean Drilling Program,*  
1331 *Initial Reports, 197*. College Station, TX: Ocean Drilling Program. doi:10.2973/odp.proc.ir.197.2002  
1332
- 1333 Thiede, J., Vallier, T. L. et al. (1981). *Initial Reports of the Deep Sea Drilling Project, 62*. Washington,  
1334 DC: U.S. Government Printing Office.  
1335
- 1336 Tobin, S.T., Ward, P. D., Steig, E.J., Olivero, E.B., Hilburn, I.A., Mitchell, R.N., Diamond, M. R., Raub,  
1337 T.D., & Kirschvink, J. L. (2012). Extinction patterns,  $\delta^{18}O$  trends, and magnetostratigraphy from a  
1338 southern high-latitude Cretaceous–Paleogene section: Links with Deccan volcanism: *Palaeogeography,*  
1339 *Palaeoclimatology, Palaeoecology, v. 350–352, 180–188*.  
1340
- 1341 Tucholke, B. E., Vogt, P.R. et al. (1979). *Initial Reports of the Deep Sea Drilling Project, 43*. Washington,  
1342 DC: U.S. Government Printing Office.  
1343
- 1344 Tucholke, B.E., Sibuet, J.-C., Klaus, A. et al. (2004). *Proceedings of the Ocean Drilling Program,*  
1345 *Scientific Results, 210*. College Station, TX: Ocean Drilling Program. doi:10.2973/odp.proc.ir.210.2004  
1346
- 1347 van Hinte, J. E., Wise, Jr., S.W. et al. (1987). *Initial Reports of the Deep Sea Drilling Project, 93*.  
1348 Washington, DC: U.S. Government Printing Office.  
1349
- 1350 Veevers, J. J., Heirtzler, J.R. et al. (1974). *Initial Reports of the Deep Sea Drilling Project, 27*.  
1351 Washington, DC: U.S. Government Printing Office.  
1352
- 1353 von der Borch, C., Sclater, C.J.G. et al. (1974). *Initial Reports of the Deep Sea Drilling Project, 22*.  
1354 Washington, DC: U.S. Government Printing Office.  
1355

1356 von Rad, U., Ryan, W.B.F. et al. (1979). *Initial Reports of the Deep Sea Drilling Project, 47, Part 1.*  
1357 Washington, DC: U.S. Government Printing Office.  
1358

1359 von Rad, U., Haq, B.U. et al. (1992). *Proceedings of the Ocean Drilling Program, Scientific Results, 122.*  
1360 College Station, TX: Ocean Drilling Program.  
1361

1362 Weissel, J., Peirce, J., Taylor, E., Alt, J. et al. (1991). *Proceedings of the Ocean Drilling Program,*  
1363 *Scientific Results, 121.* College Station, TX: Ocean Drilling Program.  
1364

1365 Winterer, E.L., Ewing, J.I. et al. (1973). *Initial Reports of the Deep Sea Drilling Project, 17.* Washington,  
1366 DC: U.S. Government Printing Office.  
1367

1368 Wits, J.D., Whittle, R.J., Wignall, P.B., Crame, J.A., Francis, J.E., Newton, R.J., & Bowman, V. (2016).  
1369 Macrofossil evidence for a rapid and severe Cretaceous–Paleogene mass extinction in Antarctica.  
1370 *Nature Communications, 7,* 11738. doi:10.1038/ncomms11738.

1371 Wits, J.D., Newton, R.J., Mills, B.J.W., Wignall, P.B., Bottrell, S.H., Hall, J.L.O., Francis, J.E. & Crame,  
1372 J.A. (2018). The impact of the Cretaceous–Paleogene (K–Pg) mass extinction event on the global  
1373 sulfur cycle: Evidence from Seymour Island, Antarctica. *Geochimica et Cosmochimica Acta, 230,* 17-  
1374 45. <https://doi.org/10.1016/j.gca.2018.02.037>  
1375

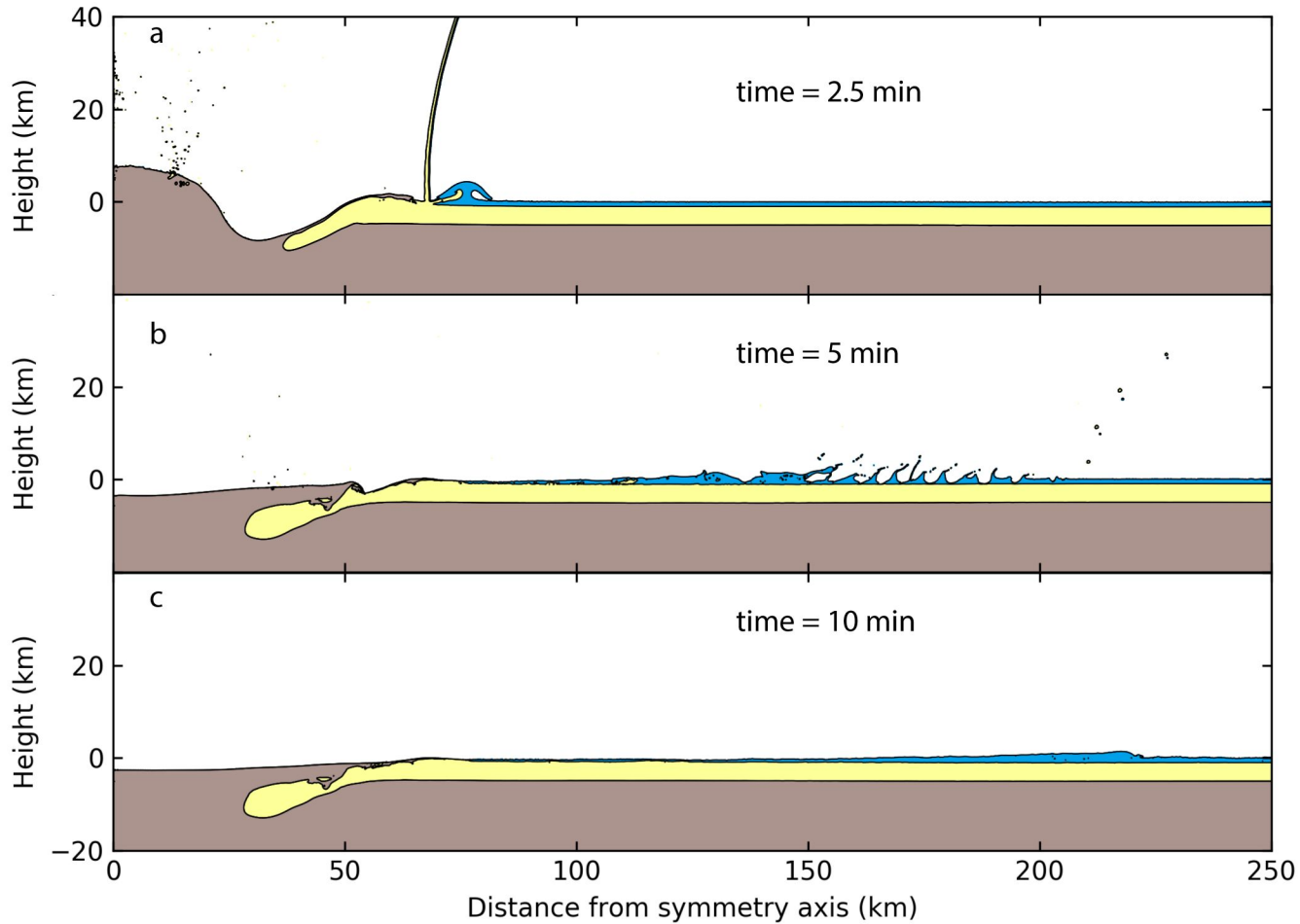
1376 Worzel, J.L., Bryant, W. et al. (1973). *Initial Reports of the Deep Sea Drilling Project, 10.* Washington,  
1377 DC: U.S. Government Printing Office.  
1378

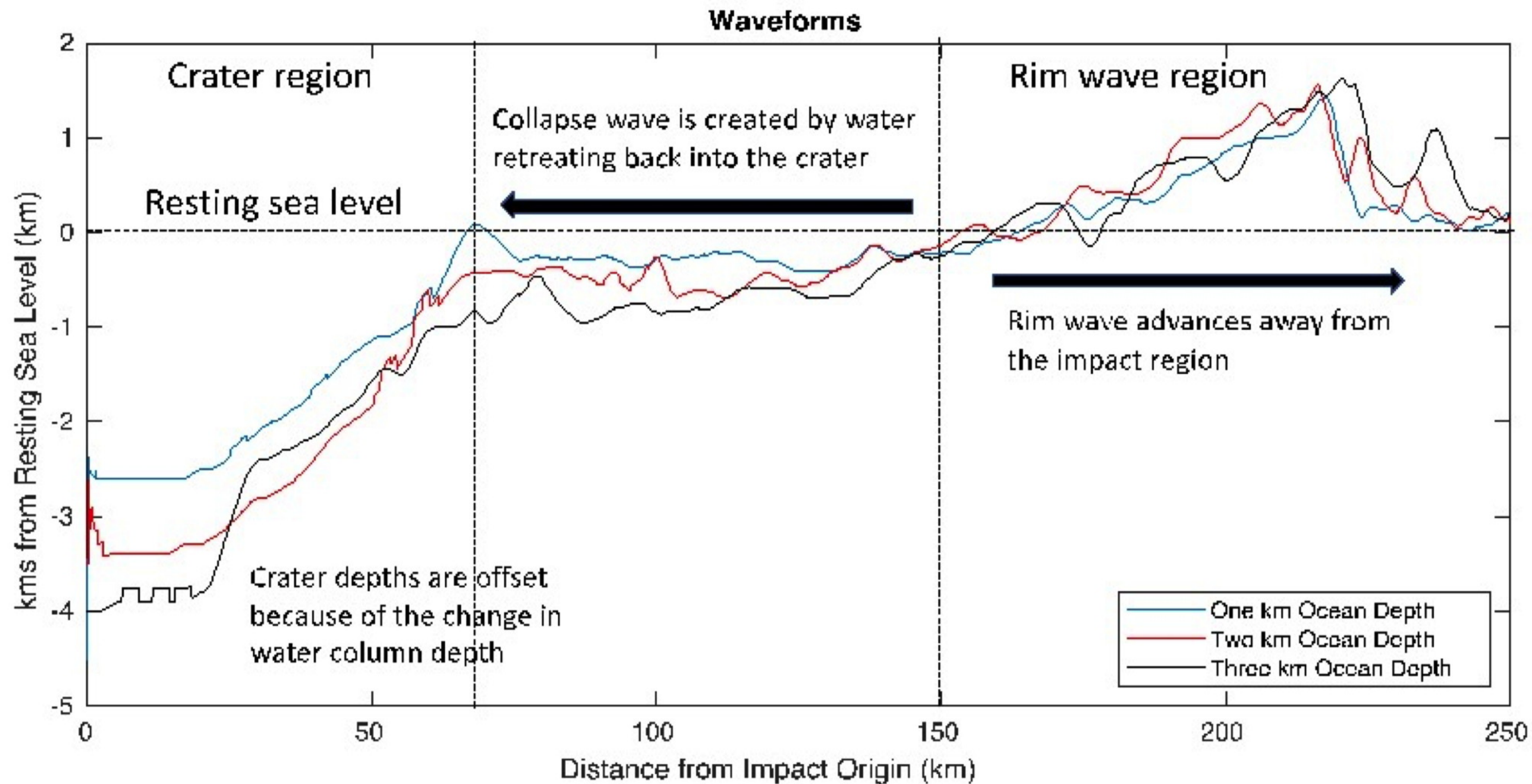
1379 Zachos, J.C., Arthur, M.A., Thunell, R.C., Williams, D.F., & Tappa, E.J. (1985). Stable isotope and trace  
1380 element geochemistry of carbonate sediments across the Cretaceous/Tertiary boundary at Deep Sea  
1381 Drilling Project Hole 577, Leg 86. In G.R. Heath, L.H. Burckle, et al., *Initial Reports of the Deep Sea*  
1382 *Drilling Project, 86.* Washington DC: U.S. Government Printing Office, 513-532.  
1383 doi:10.2973/dsdp.proc.86.120.1985  
1384

1385 Zachos, J.C., Arthur, M.A., & Dean, W.E. (1989). Geochemical evidence for suppression of pelagic  
1386 marine productivity at the Cretaceous/Tertiary boundary: *Nature, 337,* 61–64.

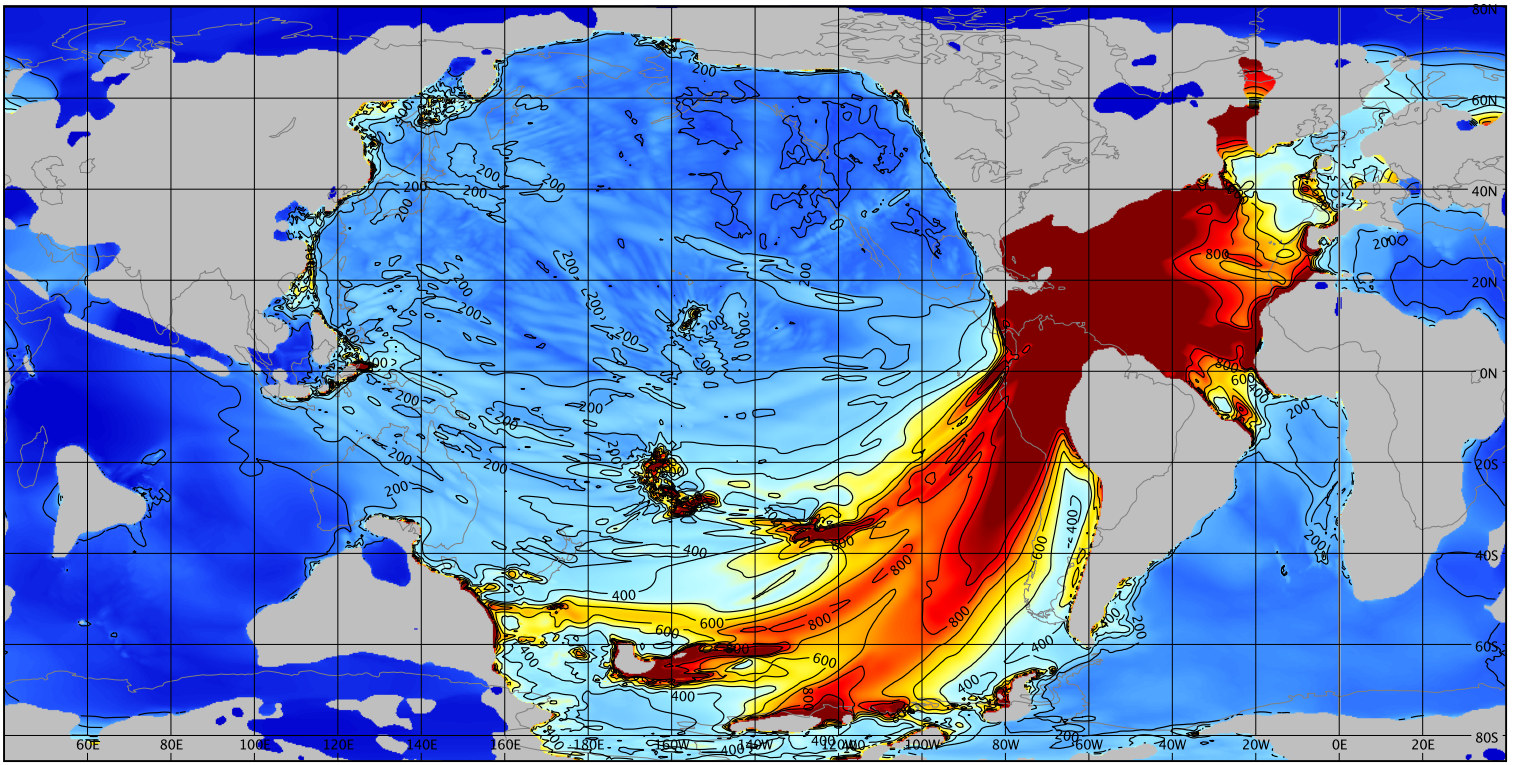
1387 Zachos, J.C., Kroon, D., Blum, P. et al. (2004). *Proceedings of the Ocean Drilling Program, Initial*  
1388 *Results 208.* College Station, TX, Ocean Drilling Program. doi:10.2973/odp.proc.ir.208.2004  
1389  
1390  
1391





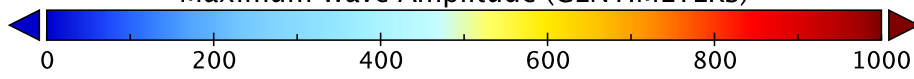


# Maximum Wave Amplitude

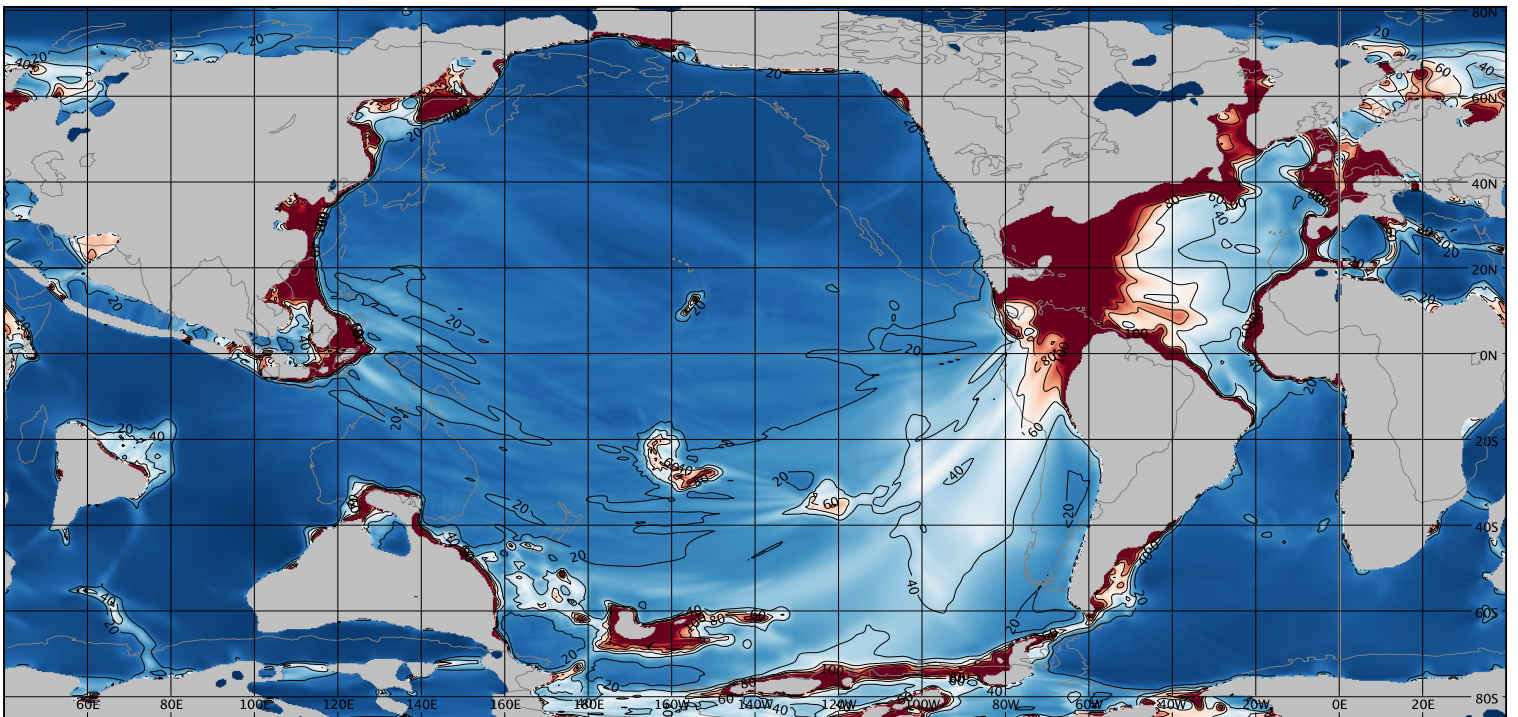


Maximum Wave Amplitude (CENTIMETERS)

(a)

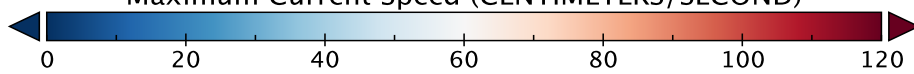


# Maximum Current Speed

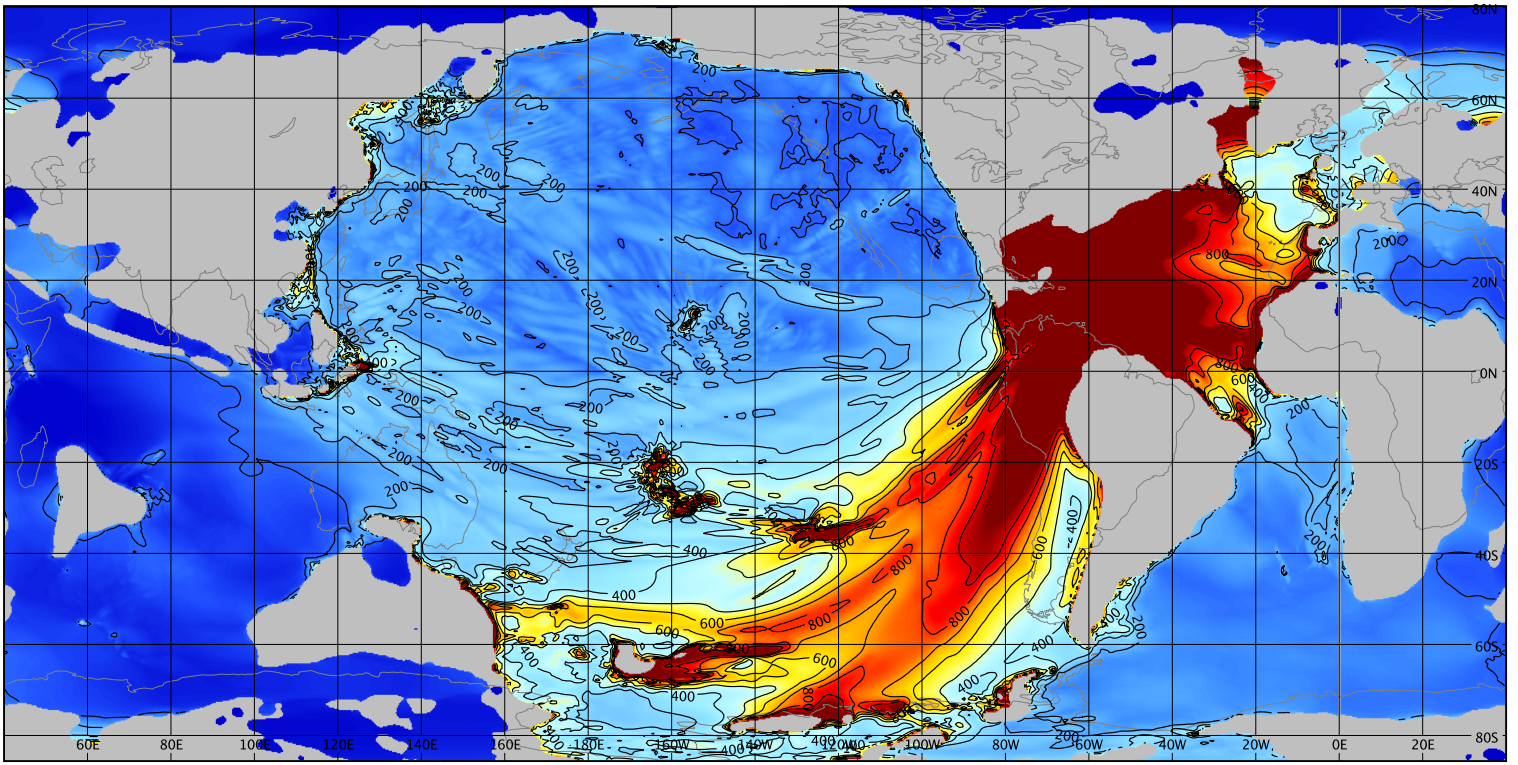


Maximum Current Speed (CENTIMETERS/SECOND)

(b)

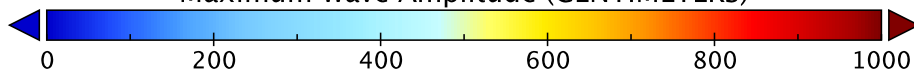


# Maximum Wave Amplitude

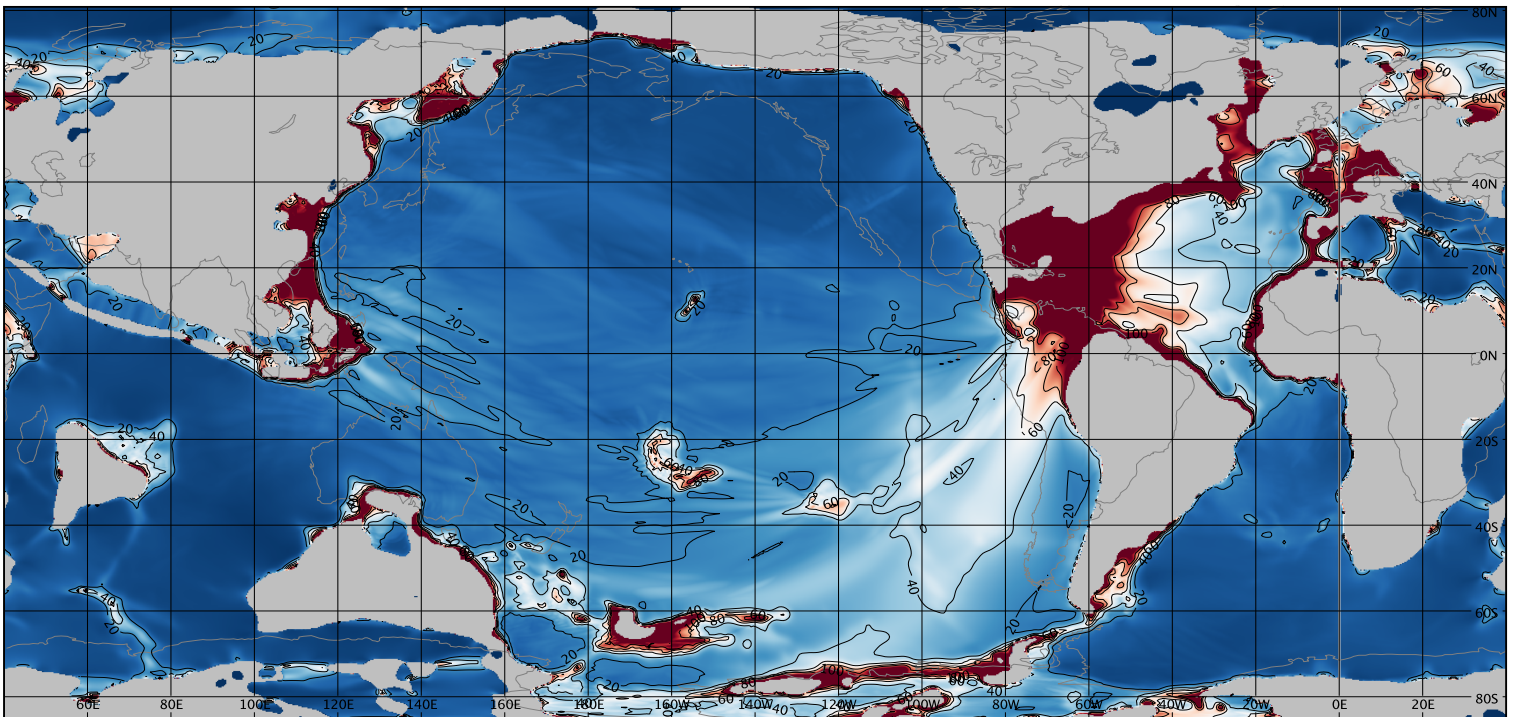


Maximum Wave Amplitude (CENTIMETERS)

(a)

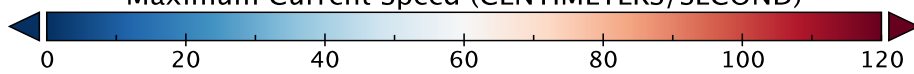


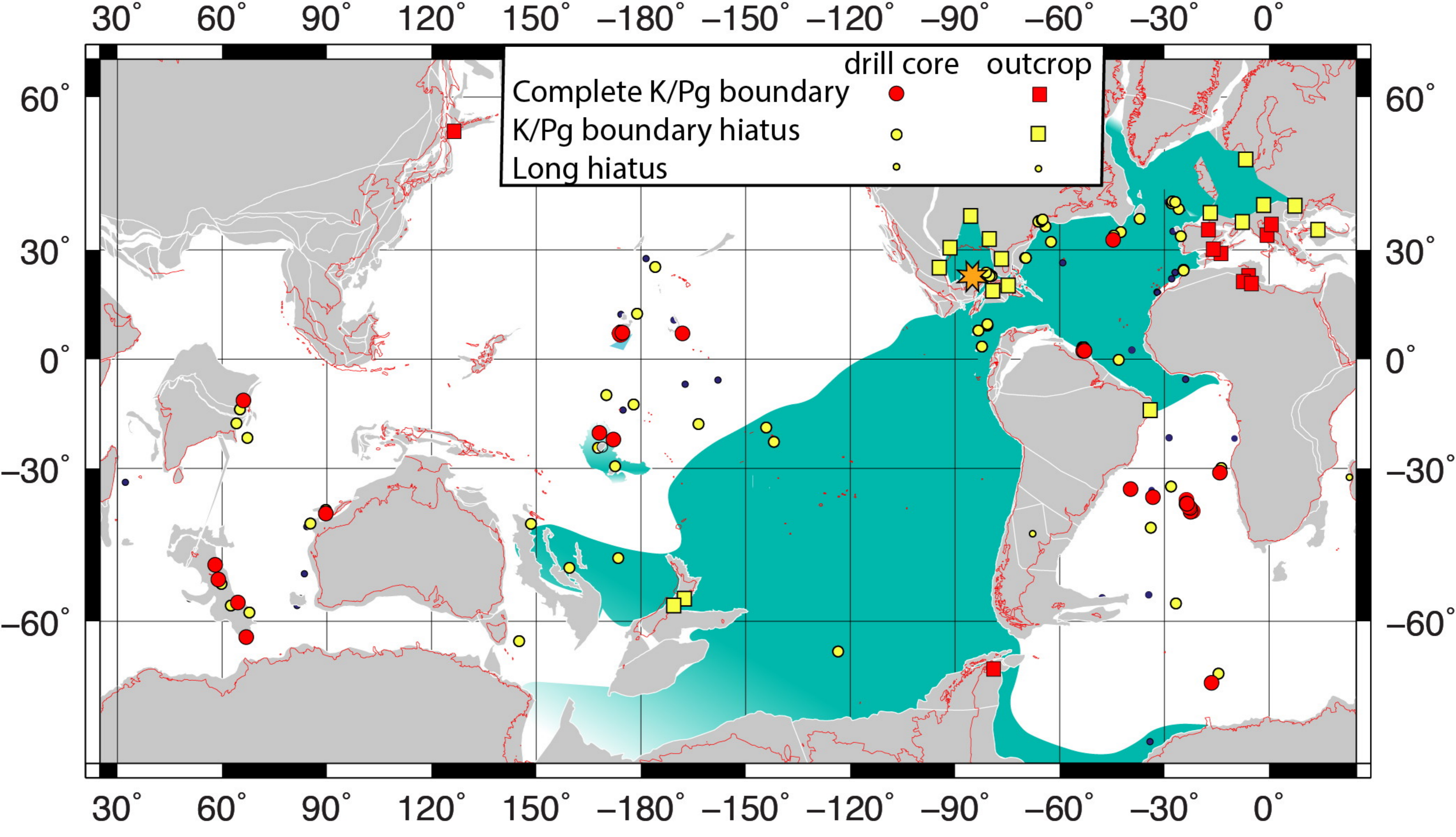
# Maximum Current Speed



Maximum Current Speed (CENTIMETERS/SECOND)

(b)





Per Cent Complete K/Pg Sections

100  
80  
60  
40  
20  
0

Caribbean

N. Atlantic

S. Atlantic

Mediterranean

N. Pacific

S. Pacific

Indian

15

35

19

9

10

18

14

